Am J Transl Res 2026;18(10):9287-9302
www.ajtr.org /ISSN:1943-8141/AJTR0175793

*Original Article*

# Antiproliferative and methylation-related effects of lycorine in myelodysplastic syndrome cells: biomarker identification, molecular docking, and cellular target-engagement analysis

Tengfei Yu[1,2,3,4*], Changting Chen[1,2*], Dangzhu Tang[4*], Yujin Li[5], Maofeng Zheng[6], Xingxia Zhang[7], Zheng Wang[8], Lihong Jiang[9], Peng Hu[3], Qianze Zhu[3,9], Tonghua Yang[1,2,3]

*[1]Faculty of Life Science and Technology, Kunming University of Science and Technology, Kunming 650500, Yunnan, China; [2]Medical School, Kunming University of Science and Technology, Kunming 650500, Yunnan, China; [3]Department of Integrated Chinese and Western Medicine, The First People's Hospital of Yunnan Province, Affiliated Hospital of Kunming University of Science and Technology, Kunming 650500, Yunnan, China; [4]Kunming Health Vocational College, Kunming 650101, China; [5]Department of Hematology, The First People's Hospital of Yunnan Province, The Affiliated Hospital of Kunming University of Science and Technology, Kunming 650500, Yunnan, China; [6]Department of Hematology, First Teaching Hospital of Tianjin University of Traditional Chinese Medicine, Tianjin 300193, China; [7]Huai'an Hospital Affiliated to Xuzhou Medical College and Huai'an Second People's Hospital, Huai'an 223022, Jiangsu, China; [8]Suzhou Jsuniwell Medical Laboratory, Suzhou 215000, Jiangsu, China; [9]Yunnan Provincial Key Laboratory of Innovative Application of Characteristic Chinese Materia Medica, The First People's Hospital of Yunnan Province, Kunming 650032, Yunnan, China. [*]Equal contributors and co-first authors.*

Received August 4, 2026; Accepted September 8, 2026; Epub October 15, 2026; Published October 30, 2026

**Abstract:** Objectives: Treatment options for myelodysplastic syndromes (MDS) remain limited. This study aimed to identify MDS-associated genes from public transcriptomic data and to evaluate the antiproliferative, target-engagement, and methylation-related effects of lycorine in MDS cell models. Methods: Public microarray datasets were analyzed by differential expression analysis, weighted gene co-expression network analysis (WGCNA), and multiple feature-selection methods. Candidate-gene expression was measured by reverse transcription-quantitative PCR (RT-qPCR) in MDS cell lines and bone marrow samples. Lycorine was evaluated by target prediction, molecular docking, cellular thermal shift assay (CETSA), Cell Counting Kit-8 (CCK-8) assay, cell-cycle and Annexin V/propidium iodide analyses, colony formation, and immunoblotting of DNA methyltransferases. Results: MIEF1 and RITA1 were consistently upregulated in public MDS datasets, SKM-1 and MUTZ-1 cells, and clinical bone marrow samples. Lycorine reduced the viability of SKM-1 and MUTZ-1 cells, with 48-h half-maximal inhibitory concentration (IC50) values of 1.74 and 4.43 μM, respectively. In SKM-1 cells, lycorine increased G2/M accumulation, and 2 μM lycorine produced a marked increase in total cell death that was driven mainly by the Annexin V-/PI+ necrotic or late-membrane-disrupted fraction. Molecular docking predicted interactions with both MIEF1 and RITA1, with a more favorable score for RITA1 (-5.20 vs. -3.17 kcal/mol). CETSA showed lycorine-associated thermal stabilization of both proteins; RITA1 displayed consistently increased soluble-protein retention and a slightly higher apparent T50 under lycorine treatment, although the estimated T50 shift was larger for MIEF1. Lycorine also reduced DNMT1, DNMT3A, and DNMT3B protein abundance, consistent with potentially reduced DNA-methylation capacity. Conclusions: MIEF1 and RITA1 are overexpressed in clinical and cellular MDS models. Lycorine inhibits MDS-cell growth, promotes cell-cycle arrest, and at 2 μM induces a predominantly necrotic or late-membrane-disrupted cell-death response. Docking and CETSA support target engagement of both MIEF1 and RITA1, with the integrated computational and thermal-stability evidence favoring RITA1. The reduction in DNMT proteins indicates reduced DNMT abundance and potentially reduced DNA-methylation capacity; DNA methylation was not measured directly.

**Keywords:** Myelodysplastic syndromes, MIEF1, RITA1, lycorine, cell-cycle arrest, cellular thermal shift assay, DNA methyltransferases

https://doi.org/10.62347/YQWT5068

## Introduction

Myelodysplastic syndromes (MDS) are clonal disorders of hematopoietic stem cells. They occur mainly in older adults and cause ineffective hematopoiesis and persistent cytopenias. Some cases progress to acute myeloid leukemia (AML) [1]. Diagnosis and risk assessment rely on morphology, cytogenetics, and molecular findings. However, the marked clinical and genetic heterogeneity of MDS remains a challenge [2]. Many patients also have few effective treatment options [2]. Additional biomarkers and candidate therapies are therefore needed [3]. Epigenetic dysregulation, including aberrant DNA methylation, is central to MDS pathogenesis, and hypomethylating agents targeting these abnormalities remain a standard of care for many patients with MDS [4].

Mitochondrial dysfunction has been reported in hematological malignancies and in disorders with epigenetic changes [5]. *MIEF1* regulates mitochondrial dynamics by recruiting DRP1 to the outer mitochondrial membrane [6].

Lycorine is an isoquinoline alkaloid found in Amaryllidaceae plants. Antitumor effects have been reported in solid and hematological cancer models [7, 8]. Depending on the model, lycorine can reduce proliferation, alter cell-cycle distribution, induce apoptotic or non-apoptotic cell death, and affect Wnt/β-catenin or TNF-α signaling [8]. It can also alter mitochondrial and epigenetic homeostasis. Some studies have reported greater activity in malignant cells than in normal cells [9]. Its effects and candidate molecular targets in MDS cells have not been established.

We first screened for genes associated with MDS and then measured the leading candidates in cell lines and bone marrow samples. We next tested whether lycorine reduced MDS-cell proliferation, altered cell-cycle and cell-death profiles, engaged the candidate proteins MIEF1 and RITA1, and affected the abundance of DNA methyltransferases. Docking and CETSA were used as complementary target-engagement approaches, while DNMT abundance was interpreted as a methylation-related endpoint rather than a direct measurement of global DNA methylation.

## Methods

### *Data sources*

We obtained MDS expression datasets from the Gene Expression Omnibus (GEO). GSE58831 included 159 MDS samples and 17 normal control samples and served as the training cohort. GSE4619 included 55 MDS samples and 11 control samples and served as the external validation cohort. All samples were bone marrow-derived CD34+ hematopoietic cells.

### *Differential expression analysis and WGCNA*

We used limma (v3.52.4) [10] to identify differentially expressed genes (DEGs) in GSE58831. The cutoffs were $|\log2 \text{ fold change}| > 0.5$ and adjusted $P < 0.05$. Heatmaps and volcano plots were prepared with pheatmap and ggplot2 [11].

We used WGCNA to identify modules associated with MDS status [12]. Samples were clustered before analysis, and outliers were removed. We selected a soft-thresholding power that produced an approximately scale-free network. Modules were defined by dynamic tree cutting. Correlations between module eigengenes and MDS status were then calculated. The module with the strongest correlation was selected for further analysis. Within this module, core genes were defined by module membership > 0.6 and gene significance > 0.2.

### *Screening of overlapping genes*

We used STRING (https://string-db.org/) to examine protein-protein associations among the candidate genes [13]. Genes present in both the DEG set and the WGCNA core-gene set were retained. Gene Ontology (GO) and Kyoto Encyclopedia of Genes and Genomes (KEGG) enrichment analyses were performed with clusterProfiler v4.4.4 [14]. Adjusted $P < 0.05$ was used as the significance cutoff.

### *Identification and verification of biomarkers*

Overlapping genes were evaluated by multiple feature-selection methods: least absolute shrinkage and selection operator (LASSO), Boruta, support vector machine-recursive fea-

ture elimination (SVM-RFE), and extreme gradient boosting (XGBoost) [15-17]. The genes selected by LASSO, SVM-RFE, and XGBoost were intersected, and the overlapping genes were designated as candidate biomarkers. Their expression and discriminatory performance were assessed in GSE58831 and GSE4619. Discrimination was summarized with receiver operating characteristic (ROC) curves. A nomogram based on the candidate genes was evaluated with calibration, ROC, and decision-curve analyses [24].

*Enrichment analysis and construction of co-expression network*

For each candidate biomarker, genes were ranked by expression correlation. Gene set enrichment analysis (GSEA) was performed with clusterProfiler v4.4.4 [14, 18]. The thresholds were |NES| > 1, nominal $P < 0.05$, and $q < 0.25$. GeneMANIA (http://genemania.org/) was used to build a co-expression network.

*Regulatory network construction*

We queried ChEA3 (https://amp.pharm.mssm.edu/ChEA3) for transcription factors linked to the candidate biomarkers and retained the top 60 results [19]. Candidate miRNAs were obtained from miRDB, miRWalk, and miRTarBase. For each biomarker, an miRNA was retained if it appeared in at least two databases. These results were combined in a TF-miRNA-mRNA network. We then used starBase to identify lncRNAs linked to the retained miRNAs. lncRNAs with clipExpNum > 25 were used to build an lncRNA-miRNA-mRNA network.

*RT-qPCR validation*

Total RNA was isolated from MUTZ-1, SKM-1, and control CD34+ cells with TRIzol (Ambion). RNA was reverse-transcribed with the SureScript First-strand cDNA Synthesis Kit (Servicebio) according to the manufacturer's protocol. Primers were designed and synthesized by Tsingke Biotechnology (Table S14). RT-qPCR was performed on a Bio-Rad platform. Relative expression was calculated by the $2^{-\Delta\Delta Cq}$ method with *GAPDH* as the reference gene.

*Clinical sample enrollment*

Bone marrow samples were obtained from 10 patients with newly diagnosed MDS and 11 healthy volunteers at Yunnan Provincial First People's Hospital between September 24, 2024, and September 23, 2025 (Table S20). Each participant or legal guardian provided written informed consent. The Ethics Committee of Yunnan Provincial First People's Hospital approved the study on September 24, 2024 (KHLL2024-KY233).

*Drug prediction and molecular docking*

Compounds associated with the candidate genes were retrieved from the Comparative Toxicogenomics Database (CTD; http://ctdbase.org/). AutoDock Vina was used to dock lycorine to APEX2, MIEF1, RITA1, and WASHC4 [20]. More negative docking scores were interpreted as more favorable predicted interactions. Docking was used to generate testable binding hypotheses and was evaluated together with CETSA rather than as proof of direct binding.

*Cell lines and culture*

Professor Qingbin Zhou (China Academy of Chinese Medical Sciences, Beijing, China) provided the SKM-1 cell line. MUTZ-1 cells were purchased from BeNa Culture Collection (Suzhou, China), and CD34+ hematopoietic cells were obtained from Yayu Biotechnology (Shanghai, China) [21, 22]. Lycorine (purity ≥ 98%; MedChemExpress; HY-N0106) was dissolved in DMSO and stored at -20°C. The final DMSO concentration was ≤ 0.1% (v/v), including in vehicle controls. CD34+ cells were maintained in StemSpan SFEM II medium supplemented with 100 ng/mL *FLT3* ligand, 100 ng/mL stem cell factor, and 50 ng/mL thrombopoietin. The cytokines were purchased from T&L Biotechnology (Beijing, China). MUTZ-1 and SKM-1 cells were maintained in RPMI-1640 containing 10% fetal bovine serum and penicillin-streptomycin (100 U/mL penicillin and 100 μg/mL streptomycin). Cells were cultured at 37°C in 5% $CO_2$.

*Cell proliferation assays*

Cell viability was measured with the Cell Counting Kit-8 (CCK-8) assay (MedChemEx-

press). Cells were seeded in 96-well plates at $8 \times 10^4$ cells per well in 100 μL of medium and exposed to lycorine (0, 1, 2, 5, 10, or 20 μM) for 24 or 48 h. CCK-8 reagent was then added at 10% of the well volume. After 1.5 h at 37°C, absorbance at 450 nm was read with a Bio-Tek Cytation 5 reader. Viability was expressed relative to the vehicle control. Half-maximal inhibitory concentration (IC50) values and 95% confidence intervals were estimated by four-parameter nonlinear regression of log concentration against normalized response. Each experiment included six technical wells per condition and was repeated in three independent experiments.

*Colony formation assay*

For the colony-formation assay, SKM-1 cells were seeded at 1,000 cells per well in 6-well plates and cultured in semisolid medium containing low-melting-point agarose (BioFroxx, cat. no. 2276GR005). Cells were exposed to 0, 0.5, 1, or 2 μM lycorine for 14 days. Colonies were fixed with 4% paraformaldehyde and stained with 0.1% crystal violet. Colony area was quantified by ImageJ-based %Area analysis of the stained wells. Three independent measurements were available, and group means were compared by one-way ANOVA.

*Cell cycle analysis*

Cells were assigned to an vehicle control, an Ara-C positive control, or one of the lycorine treatment groups. They were seeded in 12-well plates at $1.6 \times 10^6$ cells per well and treated for 48 h. For cell-cycle analysis, cells were washed with phosphate-buffered saline (PBS) and fixed overnight in 70% ethanol at -20°C. Fixed cells were collected at 1,500 × g for 5 min at 4°C and washed with PBS. The pellet was incubated in 500 μL PBS containing 5 μL RNase A for 20 min at 37°C. Cells were then stained with propidium iodide and analyzed on a NovoCyte D3000 flow cytometer. Each experiment included three technical replicates and was repeated three times.

*Apoptosis analysis*

Apoptosis was assessed by Annexin V-fluorescein isothiocyanate (FITC)/propidium iodide (PI) double staining. After 48 h of treatment, cells were collected, washed twice with phosphate-buffered saline (PBS), and resuspended in 1× binding buffer. Annexin V-FITC and PI were added, and cells were incubated for 15 min at room temperature in the dark. Stained cells were analyzed within 1 h on a NovoCyte D3000 flow cytometer. Early (Annexin V+/PI-), late (Annexin V+/PI+), and Annexin V-/PI+ (necrotic or late-membrane-disrupted) fractions were distinguished; total cell death was calculated as the sum of all three fractions. Each experiment included three technical replicates and was repeated three times.

*Western blotting assay*

Cells were lysed in RIPA buffer containing protease and phosphatase inhibitors. Protein concentration was measured with a bicinchoninic acid (BCA) assay (Proteintech). Twenty micrograms of protein per lane was separated by sodium dodecyl sulfate-polyacrylamide gel electrophoresis (SDS-PAGE) and transferred to a polyvinylidene fluoride (PVDF) membrane. Membranes were blocked for 30 min, incubated with primary antibody overnight at 4°C, and then incubated with horseradish peroxidase (HRP)-conjugated secondary antibody for 1 h at room temperature. Primary antibodies were MIEF1 (Proteintech, 20164-1-AP, lot 00134914), RITA1 (Immunoway, YT6757; ~28.6 kDa), DNMT1 (Proteintech, 24206-1-AP, lot 00149648), DNMT3A (Proteintech, 20954-1-AP, lot 00179338), DNMT3B (Proteintech, 26971-1-AP, lot 00097035), and GAPDH (Servicebio, GB11002). MIEF1, RITA1, DNMT1, DNMT3A, and DNMT3B antibodies were diluted 1:1,000; the GAPDH antibody was diluted 1:5,000. Goat anti-rabbit IgG-HRP (Servicebio, GN23303) was used at 1:5,000. Bands were detected with a Tanon 5200 imaging system and quantified in ImageJ.

*Cellular thermal shift assay (CETSA)*

CETSA was performed as described previously with minor modifications [23]. SKM-1 cells were lysed, and the protein concentration of the lysates was determined. The lysates (1 mL per tube) were divided into two groups and incubated with 10 μL of 10 mM lycorine (dissolved in DMSO) or with 10 μL DMSO (vehicle control) for 2 h at 37°C, yielding a final lycorine concentration of approximately 100 μM. Each sample was then heated in a metal heat block at 37, 40, 45, 50, 55, or 60°C for 3 min,

followed by cooling on ice. Insoluble material was removed by centrifugation, and MIEF1 and RITA1 levels in the soluble fractions were assessed by western blotting, with GAPDH probed as a loading reference. Because GAPDH itself precipitated at the higher temperatures, the melt curves were not normalized to GAPDH; instead, band intensities at each temperature were expressed relative to the 37°C value of the same replicate (fraction remaining). Apparent T50 values were estimated by fitting a Boltzmann sigmoidal model to the fraction-remaining curves of each replicate. Three independent biological replicates were analyzed for each target, and the raw densitometry values are provided in the Table S21.

*Statistical analysis*

Statistical analyses were performed in GraphPad Prism 9.0. Data are reported as mean ± SD unless stated otherwise; the figure legends specify biological and technical replication. Two groups were compared with a two-sided unpaired t-test (RT-qPCR and CETSA comparisons at each temperature). CETSA melt curves were additionally evaluated by two-way ANOVA (temperature × treatment). Three or more groups were compared by one-way ANOVA followed by Dunnett's post hoc test against the vehicle control (CCK-8 viability, cell-cycle phase proportions, early-plus-late apoptotic fractions, total cell-death rates, and DNMT western-blot densitometry). IC50 values were estimated by four-parameter nonlinear regression of log concentration against normalized response, with 95% confidence intervals. The colony-formation endpoint was compared by one-way ANOVA. Technical wells were not treated as independent biological observations. Normality was not formally tested because of the small sample sizes; all tests were two-sided. $P < 0.05$ was considered statistically significant.

## Results

*Acquisition of DEGs and critical module*

We identified 874 DEGs between MDS and control samples (**Figure 1A**; Table S1). Their expression patterns are shown in **Figure 1C**. Sample clustering identified GSM1420528 as an outlier, and this sample was removed before network analysis (Figure S1A, S1B). A soft-thresholding power of 6 was used (Figure S1C). After module merging, the network contained nine co-expression modules (Figure S1D). The dark-red module had the strongest association with MDS status ($r = 0.34$, $P = 3 \times 10^{-6}$; **Figure 1B**) and contained 12,793 genes. Of these, 839 met the module-membership and gene-significance criteria and were retained (**Figure 1D**).

*Identification of overlapping genes and functional enrichment*

The overlapping genes formed a protein-protein interaction (PPI) network. *EIF4E* and *NCBP2* had the highest numbers of connections (**Figure 2A**). Intersecting the DEG and WGCNA core-gene sets yielded 37 genes (**Figure 2B**). These genes were enriched in three KEGG pathways: selenocompound metabolism, glycosphingolipid biosynthesis-globo and isoglobo series, and thiamine metabolism (**Figure 2C**). In the GO analysis, water-soluble vitamin metabolism had the smallest adjusted *P* value (**Figure 2D**). Nucleic acid phosphodiester bond hydrolysis and negative regulation of cell-cycle phase transition had the largest gene ratios (Tables S2, S3).

*Screening of four candidate biomarkers*

Multiple feature-selection methods were applied to GSE58831. LASSO retained nine genes (Figure S2A, S2B), SVM-RFE retained 26 (Figure S2C), Boruta retained eight (Figure S2D), and XGBoost was applied in parallel. Four genes were selected by all three methods shown in the Venn diagram (LASSO, SVM-RFE, and XGBoost; **Figure 3A**): *APEX2*, *MIEF1*, *RITA1*, and KIAA1033 (*WASHC4*).

In both GSE58831 and GSE4619, APEX2, MIEF1, and RITA1 expression was significantly higher in MDS samples, whereas WASHC4 expression was significantly lower (**Figure 3B**, **3C**). Each candidate yielded an area under the ROC curve above 0.70 in both datasets (Figure S3A, S3B).

The four genes were combined in a nomogram that estimated the probability of MDS (**Figure 3D**). Calibration, ROC, and decision-curve anal-

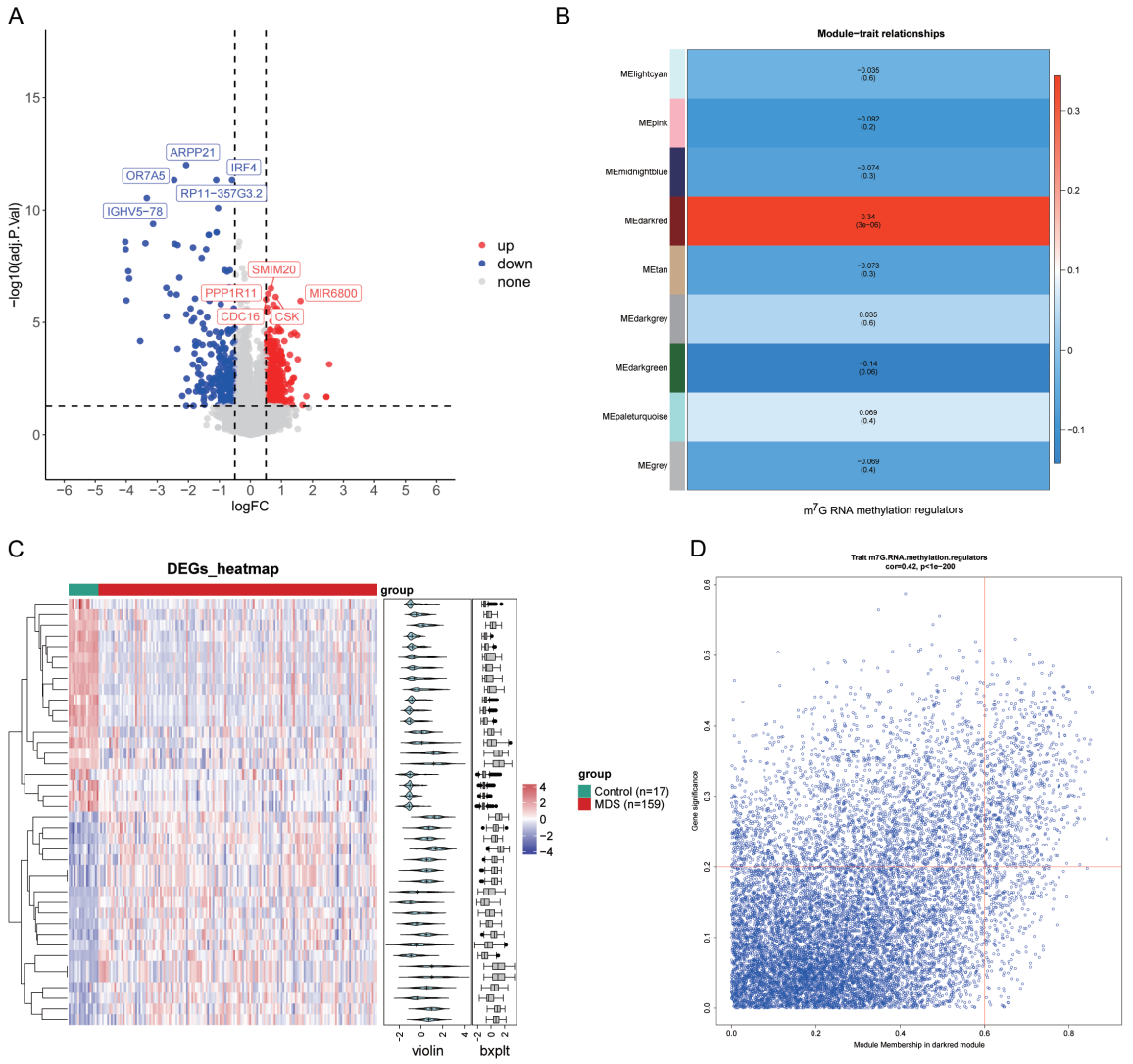



**Figure 1.** Identification of differentially expressed genes and the MDS-associated WGCNA module in GSE58831. A. Volcano plot showing upregulated (red), downregulated (blue), and non-significant (gray) genes. Dashed lines indicate the fold-change and adjusted-*P*-value thresholds. B. Module-trait correlation heatmap; each cell shows the correlation coefficient and *P* value, and the dark-red module had the strongest positive association with MDS. C. Heatmap of differentially expressed genes in control (n = 17) and MDS (n = 159) samples. D. Relationship between module membership and gene significance in the dark-red module; red reference lines indicate the screening thresholds. DEG, differentially expressed gene; GS, gene significance; MM, module membership; WGCNA, weighted gene co-expression network analysis.

yses were used to describe model performance (**Figures 3E**, **3F**, and S3C) [24].

*GSEA and co-expression network analysis of the biomarkers*

GSEA associated *APEX2*, *WASHC4*, and *RITA1* expression with pyrimidine metabolism and oxidative phosphorylation. *MIEF1* expression was associated with pyrimidine metabolism and aminoacyl-tRNA biosynthesis (Figure S4A-S4D; Tables S4, S5, S6, S7). The GeneMANIA network contained the 20 genes most closely associated with the candidates. *PDE12* had the highest degree in this network (Figure S4E).

*Regulatory networks of the biomarkers*

ChEA3 returned 211 transcription factors, of which the top 60 were included in the net-

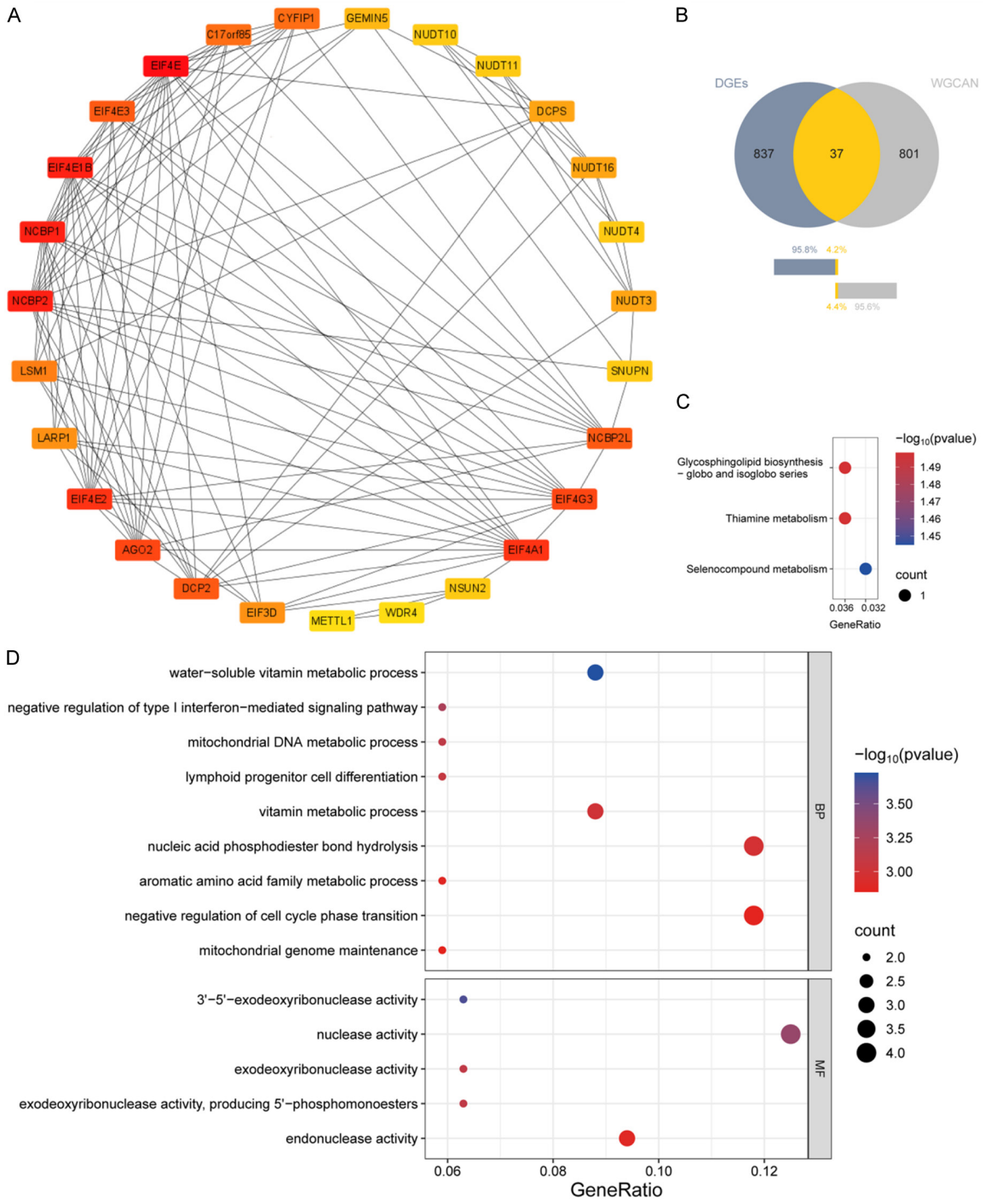



**Figure 2.** Identification and functional analysis of overlapping genes. A. Protein-protein interaction network of candidate genes; warmer node colors indicate greater network connectivity. B. Venn diagram showing 37 genes shared by the DEG and WGCNA core-gene sets. C. KEGG enrichment of the overlapping genes, including glycosphingolipid biosynthesis, thiamine metabolism, and selenocompound metabolism. D. GO enrichment bubble plots for biological process and molecular function terms; bubble size represents gene count and color represents significance. DEG, differentially expressed gene; GO, Gene Ontology; KEGG, Kyoto Encyclopedia of Genes and Genomes; PPI, protein-protein interaction; WGCNA, weighted gene co-expression network analysis.

work. The database search also identified 118 candidate miRNAs. In the resulting TF-miRNA-mRNA network, *APEX2* was linked to hsa-miR-124-3p and *ZNF317*, and *MIEF1* was linked to

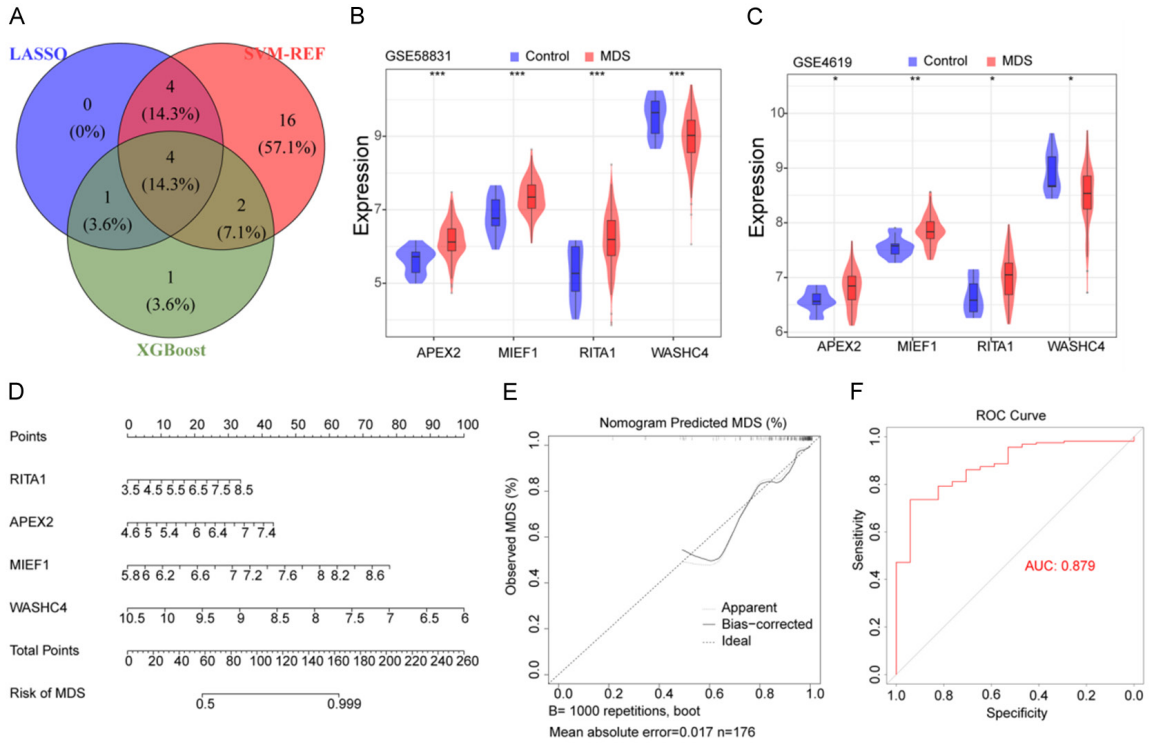



**Figure 3.** Identification and validation of candidate MDS biomarkers. (A) Intersection of genes selected by LASSO, SVM-RFE, and XGBoost, yielding four shared candidates. (B, C) Expression of APEX2, MIEF1, RITA1, and WASHC4 in GSE58831 (B) and GSE4619 (C), comparing control and MDS samples. (D) Four-gene nomogram for estimating MDS probability. (E) Calibration curve of the nomogram. (F) Receiver operating characteristic curve of the nomogram (AUC = 0.879). AUC, area under the curve; LASSO, least absolute shrinkage and selection operator; SVM-RFE, support vector machine-recursive feature elimination; XGBoost, extreme gradient boosting. *P < 0.05; **P < 0.01; ***P < 0.001.

hsa-miR-4534 and *ZBTB39* (Figure S5A; Table S8).

The starBase search returned 1,581 lncRNAs. After applying the clipExpNum > 25 filter, the retained lncRNAs were combined with the miRNA and mRNA results. In this predicted network, *WASHC4* was linked to hsa-miR-128-3p and *MIR497HG*, whereas *APEX2* was linked to hsa-miR-124-3p and *MALAT1* (Figure S5B; Table S9).

*Validation of biomarker expression in MDS cell lines and clinical samples*

RT-qPCR showed that MIEF1, RITA1, and APEX2 mRNA levels were significantly higher in both SKM-1 and MUTZ-1 MDS cell lines than in control CD34+ cells, whereas WASHC4 did not differ significantly (**Figure 4A-D**). Thus, MIEF1 and RITA1 were consistently overexpressed across both cellular MDS models.

In bone marrow samples from 10 patients with MDS and 11 healthy controls, MIEF1 and RITA1 expression was significantly higher in the MDS group (P = 0.0129 and P = 0.0002, respectively). APEX2 and WASHC4 did not differ significantly between groups (**Figure 4E-H**). Together with the cell-line data, these findings identify MIEF1 and RITA1 as the most consistently upregulated candidates in clinical and cellular MDS models.

*Drug prediction and molecular docking analysis*

The CTD search linked the candidate genes to several compounds, including apigenin, 4-phenylbutyric acid, and zalcitabine (**Figure 5**; Tables S10, S11, S12, S13). Lycorine was present in the *MIEF1*-associated compound set and was selected for further testing.

Docking predicted lycorine-binding poses for both MIEF1 and RITA1, with scores of -3.17 and

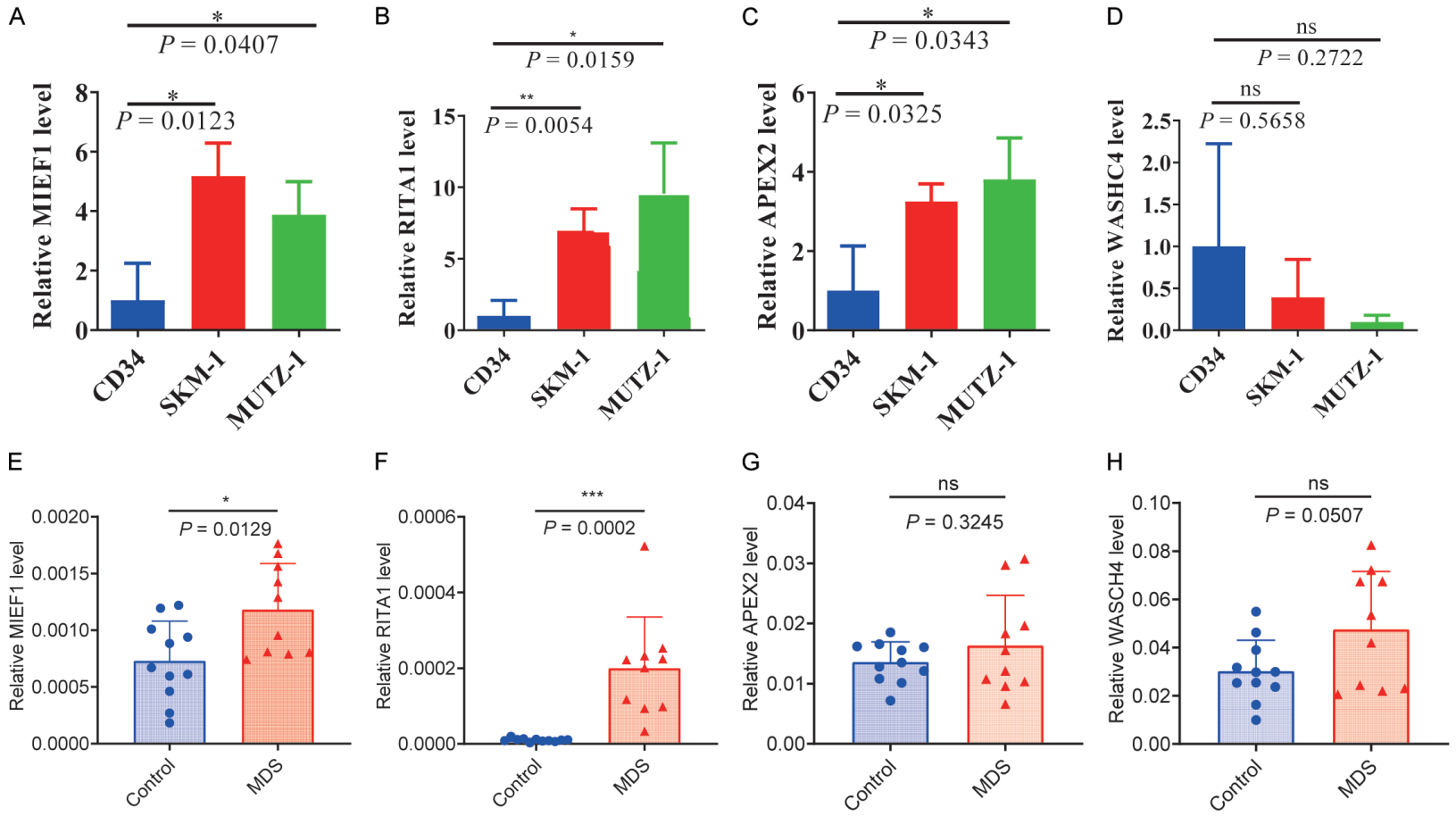



**Figure 4.** RT-qPCR validation of candidate-biomarker expression in MDS cell lines and clinical samples. (A-D) Relative mRNA levels of MIEF1 (A), RITA1 (B), APEX2 (C), and WASHC4 (D) in control CD34+ cells and the SKM-1 and MUTZ-1 MDS cell lines. (E-H) Relative expression of MIEF1 (E), RITA1 (F), APEX2 (G), and WASHC4 (H) in bone marrow samples from healthy controls (n = 11) and patients with MDS (n = 10). MIEF1 and RITA1 were significantly upregulated in both cellular and clinical MDS models. Data are presented as mean ± SD. *P < 0.05; **P < 0.01; ***P < 0.001; ns, not significant.

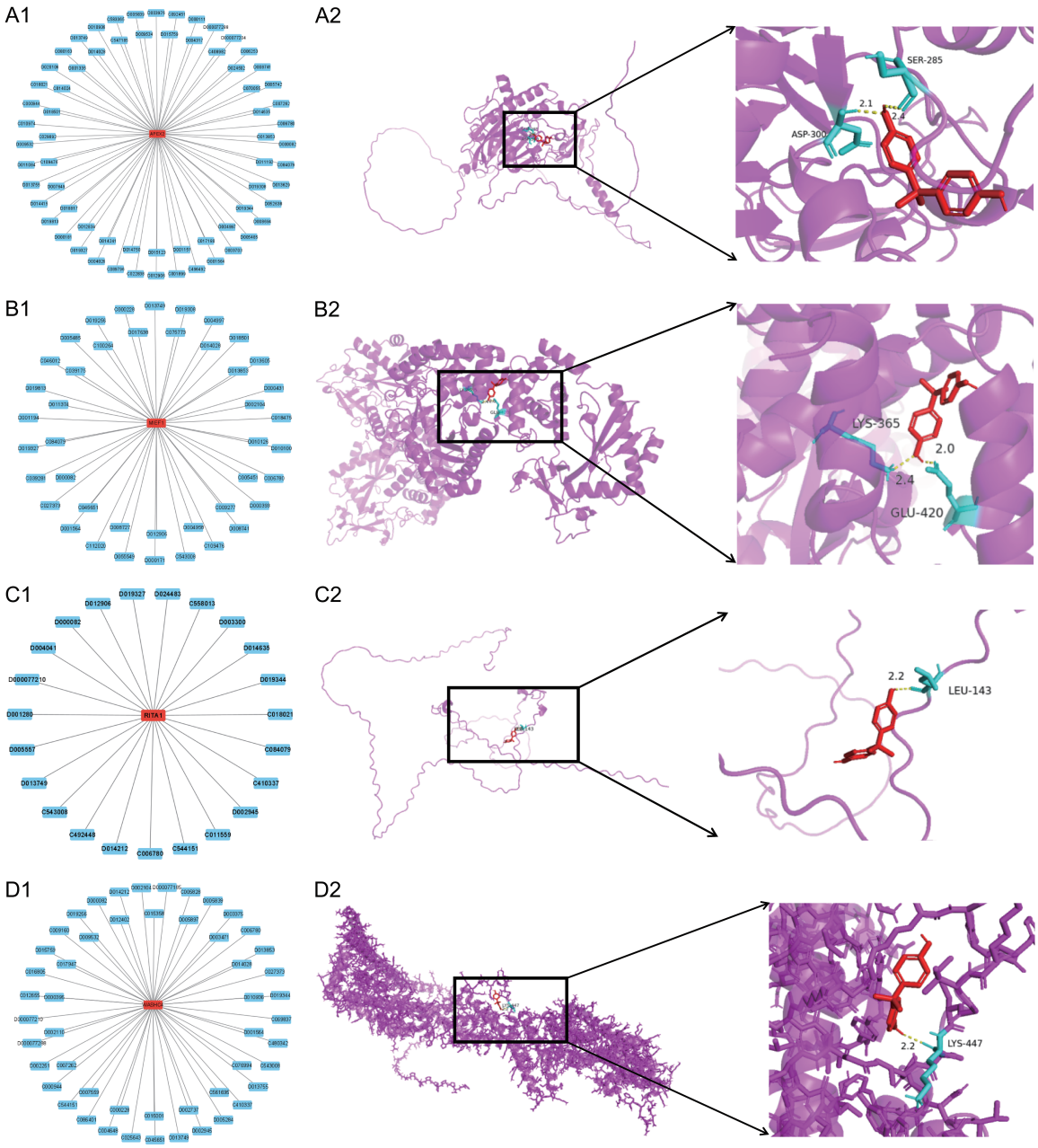



**Figure 5.** Drug-gene interaction networks and predicted lycorine docking poses for four MDS biomarkers. (A1 to D1) CTD-derived compound networks for APEX2 (A1), MIEF1 (B1), RITA1 (C1), and WASHC4 (D1); red nodes represent biomarker genes and blue nodes represent associated compounds. (A2 to D2) Overall protein structures and enlarged predicted lycorine-binding sites for APEX2, MIEF1, RITA1, and WASHC4, respectively. Proteins are shown in purple, lycorine in red, and interacting residues in cyan; yellow dashed lines and numerical labels indicate predicted interactions and distances in Å. The docking scores for MIEF1 and RITA1 were -3.17 and -5.20 kcal/mol, respectively, indicating a more favorable predicted interaction with RITA1. CTD, Comparative Toxicogenomics Database. Docking poses are hypothesis-generating and do not alone establish direct binding.

-5.20 kcal/mol, respectively (**Figure 5B2** and **5C2**). The more negative score for RITA1 indicates a more favorable predicted interaction than for MIEF1. The CTD-derived compound networks and predicted docking poses for APEX2, MIEF1, RITA1, and WASHC4 are shown in **Figure 5A1**, **5A2**, **5B1**, **5B2**, **5C1**, **5C2** and **5D1**, **5D2**, respectively. Both proteins were

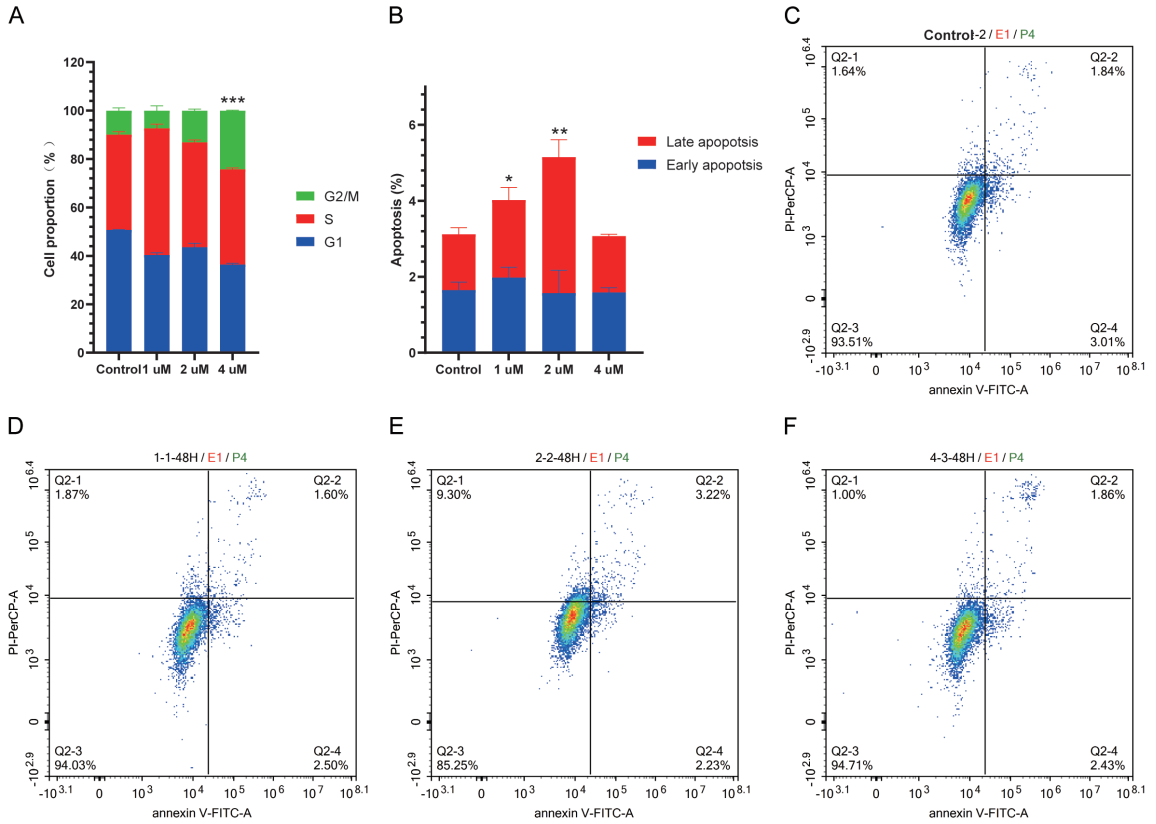



**Figure 6.** Lycorine induces cell-cycle arrest and cell death in SKM-1 MDS cells. (A) Cell-cycle distribution after 48 h of treatment with 0, 1, 2, or 4 μM lycorine. Lycorine increased the G2/M fraction, with a significant increase at 4 μM. (B) Early- and late-apoptotic fractions measured by Annexin V-FITC/PI staining. (C-F) Representative Annexin V-FITC/PI dot plots for the vehicle control (C) and 1 μM (D), 2 μM (E), and 4 μM (F) lycorine groups. The upper-left quadrant represents Annexin V-/PI+ necrotic or late-membrane-disrupted cells; this fraction was markedly increased at 2 μM. Panel B shows the early-plus-late apoptotic fraction only; the 25.38% total cell-death value reported in the Results additionally includes the Annexin V-/PI+ population. For panels A and B, significance symbols indicate one-way ANOVA followed by Dunnett's multiple-comparisons test versus the vehicle control. Data are presented as mean ± SD. *P < 0.05; **P < 0.01; ***P < 0.001; ns, not significant. FITC, fluorescein isothiocyanate; PI, propidium iodide.

therefore taken forward for CETSA. These docking results support potential interactions but do not, by themselves, prove direct binding.

*Lycorine inhibits the proliferation of MDS cells in vitro*

Lycorine reduced CCK-8 viability in both MDS cell lines across the tested concentration range (Table S17). The 48-h IC50 was 1.74 μM in SKM-1 cells and 4.43 μM in MUTZ-1 cells. SKM-1, the more sensitive line, was used for subsequent functional assays. Because SKM-1 was derived from an MDS case that progressed to acute monocytic leukemia, these results should be interpreted with that biological context in mind.

*Effects of lycorine on cell cycle distribution and apoptosis*

After 48 h of treatment, lycorine caused dose-dependent G2/M accumulation in SKM-1 cells. The G2/M fraction increased from 9.90% ± 2.03% in the vehicle control to 13.10% ± 1.16% at 2 μM (P = 0.077) and 24.22% ± 0.41% at 4 μM (P < 0.001; **Figure 6A**; Table S18), demonstrating cell-cycle arrest at the higher concentration. Ara-C induced S-phase accumulation, confirming the responsiveness of the assay.

Annexin V-FITC/PI analysis distinguished viable, early-apoptotic, late-apoptotic, and Annexin V-/PI+ necrotic or late-membrane-disrupted

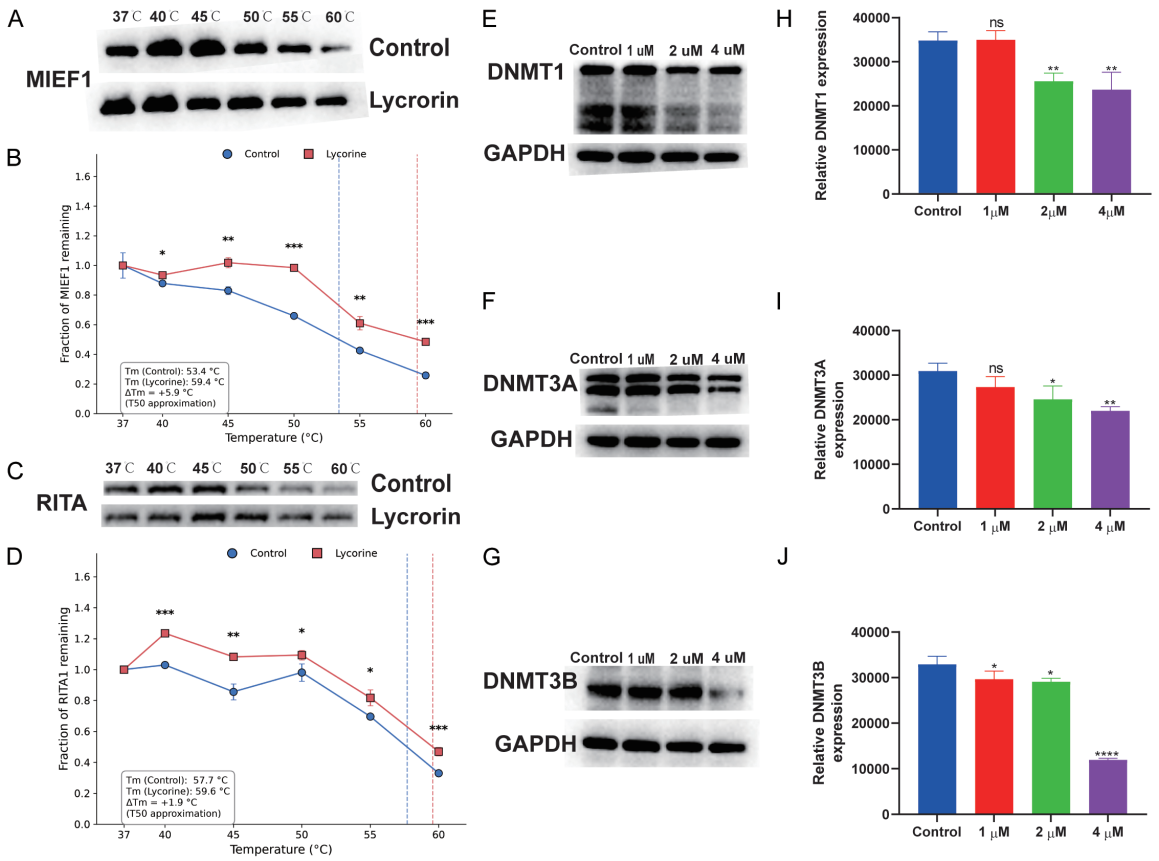



**Figure 7.** Lycorine-associated thermal stabilization of MIEF1 and RITA1 and reduced DNA methyltransferase abundance in SKM-1 cells. (A) Representative CETSA immunoblots for MIEF1 in lysates incubated with vehicle or lycorine across 37-60 °C. (B) MIEF1 fraction remaining relative to 37 °C; the apparent T50 values were 53.4 °C for vehicle and 59.4 °C for lycorine (ΔT50 ≈ +5.9 °C). (C) Representative CETSA immunoblots for RITA1 across 37-60 °C. (D) RITA1 fraction remaining relative to 37 °C; the apparent T50 values were 57.7 °C for vehicle and 59.6 °C for lycorine (ΔT50 ≈ +1.9 °C). Lycorine increased the soluble fraction of both proteins over the temperature range, supporting target engagement. (E-G) Representative immunoblots of DNMT1 (E), DNMT3A (F), and DNMT3B (G) after 48 h of treatment with 0, 1, 2, or 4 μM lycorine; GAPDH served as the loading control. (H-J) Densitometric quantification of DNMT1 (H), DNMT3A (I), and DNMT3B (J), showing concentration-dependent reductions. Data are presented as mean ± SD. *P < 0.05; **P < 0.01; ***P < 0.001; ****P < 0.0001; ns, not significant. CETSA, cellular thermal shift assay; DNMT, DNA methyltransferase; T50, approximate temperature at which 50% of soluble protein remains.

cells. Early plus late apoptosis increased modestly at 1 and 2 μM. The clearest response occurred at 2 μM, where the Annexin V-/PI+ fraction rose to 20.24% ± 12.37% from 1.60% ± 0.45% in the vehicle group. Consequently, total cell death increased from 4.71% ± 0.74% in the vehicle group to 25.38% ± 12.28% at 2 μM (overall one-way ANOVA P = 0.0085; **Figure 6B-F**; Table S19).

These data show that 2 μM lycorine induces a substantial cell-death response in SKM-1 cells, dominated by the Annexin V-/PI+ fraction rather than classical Annexin V-positive apoptosis. Because Annexin V-/PI+ events may represent primary necrosis or late membrane disruption and varied among replicates, the response is described as predominantly necrotic or late-membrane-disrupted cell death rather than pure apoptosis.

*Colony formation assay in SKM-1 cells*

After 14 days, ImageJ-based %Area analysis of crystal-violet-stained colonies showed that colony formation was significantly reduced in the 2 μM group compared with control (P < 0.05), whereas the 0.5 and 1 μM groups did not differ significantly from control (Figure S6; Table S16).

*Lycorine engages MIEF1 and RITA1 and suppresses DNA methyltransferase abundance*

CETSA was used to assess lycorine-associated changes in the thermal stability of MIEF1 and RITA1 in SKM-1 cell lysates. The soluble fraction of each protein was expressed relative to its 37°C value. Lycorine shifted the apparent thermal-transition curves of both proteins toward higher temperatures (**Figure 7A-D**; Table S21). The figure-derived T50 approximations were 53.4°C for vehicle and 59.4°C for lycorine-treated MIEF1 (ΔT50 ≈ +5.9°C) and 57.7°C for vehicle and 59.6°C for lycorine-treated RITA1 (ΔT50 ≈ +1.9°C). RITA1 showed consistently greater soluble-protein retention with lycorine from 40 to 60°C and reached a slightly higher lycorine-associated T50 than MIEF1, whereas MIEF1 showed the larger estimated shift from its vehicle curve. Together with the more favorable RITA1 docking score, the CETSA data support engagement of both proteins and provide stronger integrated evidence for RITA1. These assays support target engagement but do not substitute for a purified-protein binding measurement.

After 48 h of lycorine treatment, DNMT1, DNMT3A, and DNMT3B protein abundance decreased in SKM-1 cells (**Figure 7E-J**; Table S15). DNMT1 and DNMT3A were significantly reduced at 2 and 4 μM, while DNMT3B decreased across the tested concentrations and showed its largest reduction at 4 μM. Because these enzymes establish and maintain cytosine methylation, their coordinated reduction indicates reduced DNMT abundance and potentially reduced DNA-methylation capacity after lycorine exposure. Global or locus-specific DNA methylation was not measured directly.

## Discussion

This study combined public transcriptomic analysis, cellular and clinical expression validation, molecular docking, CETSA, and functional assays to evaluate lycorine in MDS. MIEF1 and RITA1 were consistently upregulated in two public datasets, MDS cell lines, and patient bone marrow samples. Lycorine reduced viability in SKM-1 and MUTZ-1 cells, promoted G2/M arrest, induced a predominantly necrotic or late-membrane-disrupted cell-death response at 2 μM, engaged both MIEF1 and RITA1 in complementary docking and CETSA analyses, and reduced DNMT1, DNMT3A, and DNMT3B abundance.

The four-gene panel was selected by WGCNA followed by three feature-selection methods. All four genes showed discrimination in a second public dataset. *MIEF1* and *RITA1* were also supported by the cell-line and clinical RT-qPCR results. Published studies have linked metabolic changes to malignant phenotypes [25-30]. Our clinical set included only 10 MDS samples and 11 controls. It is sufficient for initial candidate testing, but not for diagnostic validation. Larger cohorts should include MDS subtypes and clinically relevant comparator groups.

Lycorine has shown anticancer activity in several experimental systems [7, 8, 31]. Here, it reduced CCK-8 viability in both SKM-1 and MUTZ-1 cells, with SKM-1 showing greater sensitivity. Lycorine also increased the G2/M fraction, supporting cell-cycle arrest. Although Annexin V-positive apoptosis increased only modestly, the Annexin V-/PI+ fraction rose markedly at 2 μM and produced a substantial increase in total cell death. Thus, at 2 μM, lycorine primarily promoted necrotic or late-membrane-disrupted cell death rather than classical apoptosis. Colony formation was also significantly reduced at 2 μM (Figure S6; Table S16).

Molecular docking and CETSA provided complementary evidence that lycorine can engage both MIEF1 and RITA1. The docking score was more favorable for RITA1 than for MIEF1 (-5.20 vs. -3.17 kcal/mol), supporting a stronger predicted interaction with RITA1. In CETSA, lycorine increased the apparent thermal stability of both proteins. RITA1 showed a higher soluble fraction under lycorine treatment than under vehicle treatment throughout 40-60°C and reached a slightly higher lycorine-associated apparent T50 than MIEF1. The convergence of the more favorable docking result and the consistent RITA1 thermal-retention pattern therefore favors RITA1 as the more strongly supported lycorine-interacting candidate, while MIEF1 remains a plausible additional target. Direct binding and affinity should be confirmed by purified-protein methods such as surface plasmon resonance or microscale thermophoresis.

Lycorine reduced DNMT1, DNMT3A, and DNMT3B protein abundance, with the strongest effects generally observed at 2-4 μM. Because DNMT1 maintains existing methylation patterns and DNMT3A/3B establish new methylation marks, their coordinated reduction indicates reduced DNMT abundance and potentially reduced DNA-methylation capacity after lycorine treatment. This finding provides a methylation-related mechanistic direction for MDS, in which aberrant DNA methylation is central to disease biology and therapy [4]. However, DNMT abundance is a surrogate endpoint; global and locus-specific methylation assays are needed to establish the magnitude and genomic distribution of methylation changes.

This study has several limitations. The clinical validation set was small and did not support MDS-subtype analyses. Most functional assays were performed in SKM-1 cells, and non-malignant hematopoietic cells were not included in the drug-response experiments. CETSA and docking support target engagement but do not quantify binding affinity, and genetic perturbation was not performed to establish whether MIEF1 or RITA1 mediates lycorine sensitivity. Finally, DNMT protein abundance was measured, but global or locus-specific DNA methylation was not directly quantified. These limitations define priorities for follow-up studies rather than negating the consistent expression, cell-cycle, cell-death, target-engagement, and DNMT findings observed here.

Future studies should validate lycorine across additional MDS models and non-malignant CD34+ cells, quantify direct binding to MIEF1 and RITA1, and test whether genetic perturbation of either protein changes lycorine sensitivity. Bisulfite sequencing, methylation arrays, or targeted methylation assays should be used to confirm whether the reduction in DNMT proteins translates into lower global or locus-specific DNA methylation.

Overall, the data support a multi-component model in which MIEF1 and RITA1 are overexpressed in MDS, lycorine suppresses MDS-cell growth through cell-cycle arrest and a 2 μM cell-death response, both proteins can be engaged by lycorine with stronger integrated evidence for RITA1, and lycorine reduces DNMT abundance in a manner consistent with potentially reduced DNA-methylation capacity.

## Conclusions

MIEF1 and RITA1 are consistently overexpressed in clinical and cellular MDS models. Lycorine inhibits MDS-cell growth, promotes G2/M cell-cycle arrest, and at 2 μM induces predominantly necrotic or late-membrane-disrupted cell death. Molecular docking and CETSA support engagement of both MIEF1 and RITA1, with the integrated evidence favoring RITA1. Lycorine also reduces DNMT1, DNMT3A, and DNMT3B abundance, indicating reduced DNMT abundance and potentially reduced DNA-methylation capacity. These findings support further preclinical evaluation of lycorine and direct validation of its protein targets and epigenetic effects in MDS.

## Acknowledgements

This work was supported by the Hu Yu Expert Workstation (202305AF150149); the Yunnan Province Pilot Project for Clinical Collaboration in Major Difficult Diseases of Chinese and Western Medicine-Leukemia; the Yunnan Province Clinical Research Center for Hematologic Disease; the Yunnan Provincial Atherosclerosis Integrated Traditional Chinese and Western Medicine Collaborative Center; the Yunnan Provincial Clinical Medical Center for Blood Diseases and Thrombosis Prevention and Treatment; the Science and Technology Plan Project of Yunnan Province (202403-AC100017); the Yunnan Clinical Medicine Center Research Project (2024YNLCYXZX0-255 and 2024YNLCYXZX0261); the National Natural Science Foundation of China (82004187, 82060810, and 82304945); and the Huai'an Health Commission General Research Project (HAWJ2024017). The funders had no role in the study design, data collection, analysis, interpretation, or preparation of the manuscript.

## Disclosure of conflict of interest

None.

**Address correspondence to:** Tonghua Yang and Peng Hu, Department of Integrated Chinese and

Western Medicine, The First People's Hospital of Yunnan Province, Affiliated Hospital of Kunming University of Science and Technology, Kunming 650500, Yunnan, China. E-mail: ynanblood@aliyun.com (THY); hupengkkxx@126.com (PH); Qianze Zhu, Yunnan Provincial Key Laboratory of Innovative Application of Characteristic Chinese Materia Medica, The First People's Hospital of Yunnan Province, Kunming 650032, Yunnan, China. E-mail: zhuqian_ze@163.com

## References

[1] Cazzola M and Malcovati L. Myelodysplastic syndromes--coping with ineffective hematopoiesis. N Engl J Med 2005; 352: 536-538.

[2] Bewersdorf JP, Mina A, Stahl M and Zeidan AM. A 2026 update on myelodysplastic neoplasms: current state, challenges and future directions. Nat Rev Clin Oncol 2026; 23: 481-500.

[3] Zhang X, Li G, Oliverio A, VanOudenhove J, DeZern AE, Ghiaur G, Halene S, Grimes HL and Salomonis N. Clonal dissection of MDS and secondary AML resolves shared splicing neoantigens and mechanistic underpinnings of hypomethylating agent therapeutic response. Blood 2024; 144 Suppl 1: 1810.

[4] Möröy T and Khandanpour C. Role of GFI1 in epigenetic regulation of MDS and AML pathogenesis: mechanisms and therapeutic implications. Front Oncol 2019; 9: 824.

[5] Iyer P, Jasdanwala SS, Bhatia K and Bhatt S. Mitochondria and acute leukemia: a clinician's perspective. Int J Mol Sci 2024; 25: 9704.

[6] Yu R, Lendahl U, Nistér M and Zhao J. Regulation of mammalian mitochondrial dynamics: opportunities and challenges. Front Endocrinol (Lausanne) 2020; 11: 374.

[7] Zhang YM, Li T, Xu CC, Qian JY, Guo H, Zhang X, Zhan ZJ and Lu JJ. Uncover the anticancer potential of lycorine. Chin Med 2024; 19: 121.

[8] Roy M, Liang L, Xiao X, Feng P, Ye M and Liu J. Lycorine: a prospective natural lead for anticancer drug discovery. Biomed Pharmacother 2018; 107: 615-624.

[9] Sheng J, An Q, Yu F, Xiao Y, Ding H, Wu L, Duan G, Yangyin T, Chen H, Wang J, Yao S and Zhang Y. Lycorine suppresses DPP3-mediated Nrf2 signaling, thereby reducing SLC7A11 levels to trigger ferroptosis in colorectal cancer cells. Phytomedicine 2026; 156: 158221.

[10] Ritchie ME, Phipson B, Wu D, Hu Y, Law CW, Shi W and Smyth GK. Limma powers differential expression analyses for RNA-sequencing and microarray studies. Nucleic Acids Res 2015; 43: e47.

[11] Ito K and Murphy D. Application of ggplot2 to pharmacometric graphics. CPT Pharmacometrics Syst Pharmacol 2013; 2: e79.

[12] Langfelder P and Horvath S. WGCNA: an R package for weighted correlation network analysis. BMC Bioinformatics 2008; 9: 559.

[13] Szklarczyk D, Kirsch R, Koutrouli M, Nastou K, Mehryary F, Hachilif R, Gable AL, Fang T, Doncheva NT, Pyysalo S, Bork P, Jensen LJ and von Mering C. The STRING database in 2023: protein-protein association networks and functional enrichment analyses for any sequenced genome of interest. Nucleic Acids Res 2023; 51: D638-D646.

[14] Wu T, Hu E, Xu S, Chen M, Guo P, Dai Z, Feng T, Zhou L, Tang W, Zhan L, Fu X, Liu S, Bo X and Yu G. clusterProfiler 4.0: A universal enrichment tool for interpreting omics data. Innovation (Camb) 2021; 2: 100141.

[15] Guyon I, Weston J, Barnhill S and Vapnik V. Gene selection for cancer classification using support vector machines. Machine Learning 2002; 46: 389-422.

[16] Kursa MB and Rudnicki WR. Feature selection with the Boruta package. J Stat Soft 2010; 36: 1-13.

[17] Tibshirani R. Regression shrinkage and selection via the lasso. J R Stat Soc B 1996; 58: 267-288.

[18] Subramanian A, Tamayo P, Mootha VK, Mukherjee S, Ebert BL, Gillette MA, Paulovich A, Pomeroy SL, Golub TR, Lander ES and Mesirov JP. Gene set enrichment analysis: a knowledge-based approach for interpreting genome-wide expression profiles. Proc Natl Acad Sci U S A 2005; 102: 15545-15550.

[19] Keenan AB, Torre D, Lachmann A, Leong AK, Wojciechowicz ML, Utti V, Jagodnik KM, Kropiwnicki E, Wang Z and Ma'ayan A. ChEA3: transcription factor enrichment analysis by orthogonal omics integration. Nucleic Acids Res 2019; 47: W212-W224.

[20] Trott O and Olson AJ. AutoDock Vina: improving the speed and accuracy of docking with a new scoring function, efficient optimization, and multithreading. J Comput Chem 2010; 31: 455-461.

[21] Nakagawa T, Matozaki S, Murayama T, Nishimura R, Tsutsumi M, Kawaguchi R, Yokoyama Y, Hikiji K, Isobe T and Chihara K. Establishment of a leukaemic cell line from a patient with acquisition of chromosomal abnormalities during disease progression in myelodysplastic syndrome. Br J Haematol 1993; 85: 469-476.

[22] Steube KG, Gignac SM, Hu ZB, Teepe D, Harms D, Kabisch H, Gaedicke G, Hansen-Hagge T, Macleod RA, Quentmeier H and Drexler HG. In vitro culture studies of childhood myelodys-

plastic syndrome: establishment of the cell line MUTZ-1. Leuk Lymphoma 1997; 25: 345-363.
[23] Jafari R, Almqvist H, Axelsson H, Ignatushchenko M, Lundbäck T, Nordlund P and Martinez Molina D. The cellular thermal shift assay for evaluating drug target interactions in cells. Nat Protoc 2014; 9: 2100-2122.
[24] Iasonos A, Schrag D, Raj GV and Panageas KS. How to build and interpret a nomogram for cancer prognosis. J Clin Oncol 2008; 26: 1364-1370.
[25] Tang H, Li X, Jiang L, Liu Z, Chen L, Chen J, Deng M, Zhou F, Zheng X and Liu Z. RITA1 drives the growth of bladder cancer cells by recruiting TRIM25 to facilitate the proteasomal degradation of RBPJ. Cancer Sci 2022; 113: 3071-3084.
[26] Kamerkar SC, Liu A and Higgs HN. Mitochondrial fission - changing perspectives for future progress. J Cell Sci 2025; 138: jcs263640.
[27] Martell E, Kuzmychova H, Grewal A, Chawla U, Jain C, Anderson CM and Sharif T. Exploiting metabolic dependencies for therapeutic targeting of brain cancers. Cancer Lett 2026; 646: 218426.
[28] Nie Y, Yun X, Zhang Y and Wang X. Targeting metabolic reprogramming in chronic lymphocytic leukemia. Exp Hematol Oncol 2022; 11: 39.
[29] Zhao S, Zhang X, Shi Y, Cheng L, Song T, Wu B, Li J and Yang H. MIEF2 over-expression promotes tumor growth and metastasis through reprogramming of glucose metabolism in ovarian cancer. J Exp Clin Cancer Res 2020; 39: 286.
[30] Guo X, Can C, Liu W, Wei Y, Yang X, Liu J, Jia H, Jia W, Wu H and Ma D. Mitochondrial transfer in hematological malignancies. Biomark Res 2023; 11: 89.
[31] Liang X, Fu W, Peng Y, Duan J, Zhang T, Fan D, Hong W, Qi X, Wu C, He Y, Yu W, Zhou J, Guo P, Bai H and Zhang Q. Lycorine induces apoptosis of acute myeloid leukemia cells and inhibits triglyceride production via binding and targeting FABP5. Ann Hematol 2023; 102: 1073-1086.

**Table S1.** Top 50 differentially expressed genes (DEGs) between MDS and control groups in GSE58831 (|log2FC| > 0.5, adjusted P < 0.05). Full list of 874 DEGs is available upon request

| Gene Symbol | log2FC | AveExpr | t value | *P* value | adj.P.Val | B |
|---|---|---|---|---|---|---|
| ARPP21 | -2.0702 | 2.9789 | -9.3526 | 4.11e-17 | 1.00e-12 | 27.9746 |
| IRF4 | -0.5893 | 2.6453 | -8.9256 | 5.93e-16 | 4.77e-12 | 25.4401 |
| OR7A5 | -2.4564 | 2.8711 | -8.9055 | 6.73e-16 | 4.77e-12 | 25.3213 |
| RP11-357G3.2 | -1.1025 | 3.4195 | -8.8813 | 7.81e-16 | 4.77e-12 | 25.1791 |
| IGHV5-78 | -3.3390 | 3.3881 | -8.5499 | 6.00e-15 | 2.93e-11 | 23.2433 |
| GPR176 | -1.0419 | 3.0982 | -8.3530 | 1.99e-14 | 8.09e-11 | 22.1071 |
| AKAP12 | -3.1361 | 4.0322 | -8.0515 | 1.22e-13 | 4.24e-10 | 20.3879 |
| MIR631 | -1.0919 | 3.6341 | -7.8665 | 3.64e-13 | 9.88e-10 | 19.3466 |
| NEIL1 | -1.0919 | 3.6341 | -7.8665 | 3.64e-13 | 9.88e-10 | 19.3466 |
| LOC101927705 | -1.3419 | 3.1993 | -7.7877 | 5.79e-13 | 1.29e-09 | 18.9061 |
| P4HA2 | -1.3419 | 3.1993 | -7.7877 | 5.79e-13 | 1.29e-09 | 18.9061 |
| MME | -4.0307 | 4.8106 | -7.6375 | 1.39e-12 | 2.62e-09 | 18.0732 |
| RAG2 | -3.3833 | 3.5999 | -7.5996 | 1.74e-12 | 3.03e-09 | 17.8639 |
| SMAD7 | -2.4406 | 3.2085 | -7.5789 | 1.96e-12 | 3.19e-09 | 17.7497 |
| RAG1 | -2.3431 | 3.6167 | -7.5447 | 2.39e-12 | 3.65e-09 | 17.5622 |
| NPCDR1 | -1.8479 | 3.6599 | -7.4810 | 3.45e-12 | 4.68e-09 | 17.2128 |
| LDLRAD4 | -1.4248 | 5.4113 | -7.4405 | 4.35e-12 | 5.60e-09 | 16.9918 |
| P2RY14 | -4.0191 | 5.9607 | -7.4302 | 4.62e-12 | 5.64e-09 | 16.9359 |
| DUSP26 | -1.5704 | 3.3425 | -7.2682 | 1.17e-11 | 1.36e-08 | 16.0580 |
| INO80C | -0.8234 | 6.7264 | -7.0294 | 4.48e-11 | 4.76e-08 | 14.7823 |
| TP53INP1 | -0.6578 | 4.9790 | -7.0195 | 4.73e-11 | 4.82e-08 | 14.7302 |
| VPREB1 | -3.9319 | 5.7840 | -6.9931 | 5.48e-11 | 5.36e-08 | 14.5906 |
| LRIG1 | -0.7495 | 3.1484 | -6.9795 | 5.91e-11 | 5.56e-08 | 14.5188 |
| LOC100129447 | -2.2867 | 3.1673 | -6.8468 | 1.23e-10 | 1.04e-07 | 13.8228 |
| VPREB3 | -3.9043 | 4.7598 | -6.8247 | 1.39e-10 | 1.13e-07 | 13.7079 |
| PRCD | -0.6802 | 2.8345 | -6.6494 | 3.63e-10 | 2.77e-07 | 12.8012 |
| LINC01013 | -2.7109 | 3.8555 | -6.6346 | 3.93e-10 | 2.91e-07 | 12.7257 |
| SMIM20 | 0.6645 | 9.3097 | 6.6210 | 4.23e-10 | 3.04e-07 | 12.6558 |
| BACH2 | -2.5846 | 4.8117 | -6.5035 | 7.95e-10 | 5.25e-07 | 12.0578 |
| PPP1R11 | 0.5702 | 4.8069 | 6.5035 | 7.95e-10 | 5.25e-07 | 12.0578 |
| NPY | -2.3748 | 3.4687 | -6.4797 | 9.03e-10 | 5.81e-07 | 11.9375 |
| CSK | 0.8145 | 8.9543 | 6.4298 | 1.18e-09 | 7.39e-07 | 11.6857 |
| SH2D4B | -1.7836 | 2.7575 | -6.3912 | 1.45e-09 | 8.84e-07 | 11.4920 |
| CDC16 | 0.5047 | 9.8768 | 6.3581 | 1.72e-09 | 9.58e-07 | 11.3262 |
| EBF1 | -3.9956 | 4.9449 | -6.3305 | 1.99e-09 | 1.06e-06 | 11.1884 |
| SKIL | -1.3213 | 4.3826 | -6.3161 | 2.15e-09 | 1.10e-06 | 11.1170 |
| MIR6800 | 1.6148 | 7.2406 | 6.3082 | 2.24e-09 | 1.12e-06 | 11.0777 |
| CD79B | -0.9556 | 3.9799 | -6.2369 | 3.26e-09 | 1.56e-06 | 10.7243 |
| MTR | 0.7461 | 9.3492 | 6.2246 | 3.48e-09 | 1.63e-06 | 10.6635 |
| CCDC134 | 0.5421 | 4.1329 | 6.1588 | 4.90e-09 | 2.26e-06 | 10.3401 |
| MED25 | 0.8596 | 5.4608 | 6.1426 | 5.32e-09 | 2.41e-06 | 10.2608 |
| HMHB1 | -1.9262 | 3.0575 | -6.1375 | 5.46e-09 | 2.41e-06 | 10.2362 |
| HMGN2P9 | -0.5322 | 3.6777 | -6.1319 | 5.63e-09 | 2.41e-06 | 10.2085 |
| ND2 | 0.8208 | 14.4559 | 6.1003 | 6.62e-09 | 2.79e-06 | 10.0548 |
| LEF1-AS1 | -1.6181 | 3.2787 | -6.0411 | 8.98e-09 | 3.56e-06 | 9.7673 |
| TRAM2 | 0.5422 | 5.1059 | 6.0398 | 9.04e-09 | 3.56e-06 | 9.7608 |

| | | | | | | |
|---|---|---|---|---|---|---|
| NID2 | -2.0666 | 3.8673 | -5.9869 | 1.19e-08 | 4.39e-06 | 9.5056 |
| BLK | -0.6935 | 2.4842 | -5.9709 | 1.29e-08 | 4.69e-06 | 9.4289 |
| LYL1 | 1.0008 | 10.4756 | 5.9465 | 1.46e-08 | 5.22e-06 | 9.3117 |
| HEY1 | -0.8397 | 2.8133 | -5.9409 | 1.50e-08 | 5.23e-06 | 9.2849 |

Note: A total of 874 DEGs were identified. Only the top 50 ranked by adjusted *P* value are shown. Full dataset available in the supplementary data file.

**Table S2.** Top 20 Gene Ontology (GO) enrichment terms of overlapping genes

| Ontology | GO ID | Description | GeneRatio | BgRatio | *P* value | P adjust | Count |
|---|---|---|---|---|---|---|---|
| BP | GO:0006767 | water-soluble vitamin metabolic process | 3/34 | 62/18903 | 1.87e-04 | 1.87e-04 | 3 |
| BP | GO:0060339 | negative regulation of type I interferon | 2/34 | 20/18903 | 5.85e-04 | 5.85e-04 | 2 |
| BP | GO:0032042 | mitochondrial DNA metabolic process | 2/34 | 23/18903 | 7.76e-04 | 7.76e-04 | 2 |
| BP | GO:0002320 | lymphoid progenitor cell differentiation | 2/34 | 24/18903 | 8.45e-04 | 8.45e-04 | 2 |
| BP | GO:0006766 | vitamin metabolic process | 3/34 | 110/18903 | 0.0010 | 0.0010 | 3 |
| BP | GO:0090305 | nucleic acid phosphodiester bond hydroly | 4/34 | 253/18903 | 0.0011 | 0.0011 | 4 |
| BP | GO:0009072 | aromatic amino acid family metabolic pro | 2/34 | 30/18903 | 0.0013 | 0.0013 | 2 |
| BP | GO:1901988 | negative regulation of cell cycle phase | 4/34 | 272/18903 | 0.0014 | 0.0014 | 4 |
| BP | GO:0000002 | mitochondrial genome maintenance | 2/34 | 31/18903 | 0.0014 | 0.0014 | 2 |
| BP | GO:0034599 | cellular response to oxidative stress | 4/34 | 288/18903 | 0.0017 | 0.0017 | 4 |
| BP | GO:0010948 | negative regulation of cell cycle proces | 4/34 | 318/18903 | 0.0024 | 0.0024 | 4 |
| BP | GO:0060338 | regulation of type I interferon-mediated | 2/34 | 41/18903 | 0.0025 | 0.0025 | 2 |
| BP | GO:0051168 | nuclear export | 3/34 | 165/18903 | 0.0032 | 0.0032 | 3 |
| BP | GO:0062197 | cellular response to chemical stress | 4/34 | 345/18903 | 0.0033 | 0.0033 | 4 |
| BP | GO:0000075 | cell cycle checkpoint signaling | 3/34 | 186/18903 | 0.0045 | 0.0045 | 3 |
| BP | GO:0045786 | negative regulation of cell cycle | 4/34 | 405/18903 | 0.0058 | 0.0058 | 4 |
| BP | GO:0006081 | cellular aldehyde metabolic process | 2/34 | 70/18903 | 0.0070 | 0.0070 | 2 |
| BP | GO:0006979 | response to oxidative stress | 4/34 | 434/18903 | 0.0074 | 0.0074 | 4 |
| BP | GO:0060337 | type I interferon signaling pathway | 2/34 | 75/18903 | 0.0080 | 0.0080 | 2 |
| BP | GO:0045824 | negative regulation of innate immune res | 2/34 | 77/18903 | 0.0084 | 0.0084 | 2 |

Note: A total of 194 GO terms were identified. Top 20 ranked by *P* value are shown.

**Table S3.** KEGG pathway enrichment analysis of overlapping genes

| KEGG ID | Description | GeneRatio | BgRatio | *P* value | P adjust | Count |
|---|---|---|---|---|---|---|
| hsa00603 | Glycosphingolipid biosynthesis - globo and isoglob | 1/18 | 15/8386 | 0.0317 | 0.0317 | 1 |
| hsa00730 | Thiamine metabolism | 1/18 | 15/8386 | 0.0317 | 0.0317 | 1 |
| hsa00450 | Selenocompound metabolism | 1/18 | 17/8386 | 0.0359 | 0.0359 | 1 |

**Table S4.** Gene Set Enrichment Analysis (GSEA) results for APEX2 co-expressed genes (top 10 pathways ranked by adjusted *P* value, |NES| > 1, NOM P < 0.05)

| Pathway ID | Description | EnrichmentScore | NES | *P*-value | P.adjust | Rank |
|---|---|---|---|---|---|---|
| KEGG_PYRIMIDINE_METABOLIS | kegg pyrimidine metabolism | 96 | 0.631681430055969 | 2.121 | 2.591e-11 | 3.355e-09 |
| KEGG_DNA_REPLICATION | kegg dna replication | 36 | 0.760820014001903 | 2.276 | 4.489e-10 | 2.906e-08 |
| KEGG_OXIDATIVE_PHOSPHORYL | kegg oxidative phosphorylation | 109 | 0.570771689823625 | 1.933 | 3.599e-09 | 1.553e-07 |
| KEGG_PARKINSONS_DISEASE | kegg parkinsons disease | 107 | 0.557289890522774 | 1.886 | 7.182e-08 | 2.158e-06 |
| KEGG_PURINE_METABOLISM | kegg purine metabolism | 151 | 0.512102748460613 | 1.772 | 8.332e-08 | 2.158e-06 |
| KEGG_HUNTINGTONS_DISEASE | kegg huntingtons disease | 163 | 0.494474787873538 | 1.719 | 2.006e-07 | 4.329e-06 |
| KEGG_HOMOLOGOUS_RECOMBIN | kegg homologous recombination | 26 | 0.738976445915261 | 2.085 | 8.246e-07 | 1.526e-05 |
| KEGG_CELL_CYCLE | kegg cell cycle | 123 | 0.516422479380863 | 1.769 | 9.856e-07 | 1.596e-05 |
| KEGG_AMINOACYL_TRNA_BIOSY | kegg aminoacyl trna biosynthesis | 22 | 0.764304198014972 | 2.105 | 1.204e-06 | 1.733e-05 |
| KEGG_NUCLEOTIDE_EXCISION_ | kegg nucleotide excision repair | 44 | 0.645036058170205 | 1.997 | 1.826e-06 | 2.364e-05 |

Note: A total of 47 enriched pathways were identified. Top 10 shown. NES: normalized enrichment score.

**Table S5.** Gene Set Enrichment Analysis (GSEA) results for WASHC4 co-expressed genes (top 10 pathways ranked by adjusted *P* value, |NES| > 1, NOM P < 0.05)

| Pathway ID | Description | Enrich-mentScore | NES | *P*-value | P.adjust | Rank |
|---|---|---|---|---|---|---|
| KEGG_PYRIMIDINE_METABOLIS | kegg pyrimidine metabolism | 96 | -0.544834855 | -2.136 | 1.038e-08 | 1.158e-06 |
| KEGG_PARKINSONS_DISEASE | kegg parkinsons disease | 107 | -0.528775472 | -2.106 | 2.640e-08 | 1.473e-06 |
| KEGG_DNA_REPLICATION | kegg dna replication | 36 | -0.685581387 | -2.221 | 3.124e-07 | 8.714e-06 |
| KEGG_OXIDATIVE_PHOSPHORYL | kegg oxidative phosphorylation | 109 | -0.51375571 | -2.052 | 2.658e-07 | 8.714e-06 |
| KEGG_PURINE_METABOLISM | kegg purine metabolism | 151 | -0.456246061 | -1.896 | 5.914e-07 | 1.320e-05 |
| KEGG_HUNTINGTONS_DISEASE | kegg huntingtons disease | 163 | -0.446582587 | -1.872 | 8.413e-07 | 1.564e-05 |
| KEGG_PORPHYRIN_AND_CHLORO | kegg porphyrin and chlorophyll metabolis | 36 | -0.668861984 | -2.167 | 1.046-06 | 1.668e-05 |
| KEGG_PROTEASOME | kegg proteasome | 42 | -0.612768822 | -2.093 | 6.743e-06 | 9.404e-05 |
| KEGG_PHOSPHATIDYLINOSITOL | kegg phosphatidylinositol signaling syst | 76 | 0.481514817987367 | 2.055 | 9.011e-06 | 0.0001 |
| KEGG_GLYCOLYSIS_GLUCONEOG | kegg glycolysis gluconeogenesis | 60 | -0.550628948 | -1.986 | 8.480e-06 | 0.0001 |

Note: A total of 62 enriched pathways were identified. Top 10 shown. NES: normalized enrichment score.

**Table S6.** Gene Set Enrichment Analysis (GSEA) results for MIEF1 co-expressed genes (top 10 pathways ranked by adjusted *P* value, |NES| > 1, NOM P < 0.05)

| Pathway ID | Description | Enrich-mentScore | NES | *P*-value | P.adjust | Rank |
|---|---|---|---|---|---|---|
| KEGG_AUTOIMMUNE_THYROID_D | kegg autoimmune thyroid disease | 50 | -0.629215045 | -2.847 | 5.0588e-10 | 5.590e-08 |
| KEGG_GRAFT_VERSUS_HOST_DI | kegg graft versus host disease | 41 | -0.654849373 | -2.811 | 1.9188e-09 | 7.085e-08 |
| KEGG_PYRIMIDINE_METABOLIS | kegg pyrimidine metabolism | 96 | 0.593771098058164 | 2.0311 | 1.9238e-09 | 7.085e-08 |
| KEGG_AMINOACYL_TRNA_BIOSY | kegg aminoacyl trna biosynthesis | 22 | 0.810272825236663 | 2.264 | 7.7588e-09 | 2.144e-07 |
| KEGG_ALLOGRAFT_REJECTION | kegg allograft rejection | 37 | -0.64796632 | -2.736 | 4.729e-08 | 1.045e-06 |
| KEGG_CELL_CYCLE | kegg cell cycle | 123 | 0.533826204935255 | 1.868 | 7.452e-08 | 1.373e-06 |
| KEGG_CELL_ADHESION_MOLECU | kegg cell adhesion molecules cams | 130 | -0.384128719 | -2.054 | 9.518e-08 | 1.503e-06 |
| KEGG_DNA_REPLICATION | kegg dna replication | 36 | 0.710110643184528 | 2.160 | 2.02e-07 | 2.800e-06 |
| KEGG_PROTEASOME | kegg proteasome | 42 | 0.668386343507212 | 2.090 | 5.717e-07 | 7.021e-06 |
| KEGG_SPLICEOSOME | kegg spliceosome | 125 | 0.516160352614582 | 1.808 | 1.162e-06 | 1.285e-05 |

Note: A total of 62 enriched pathways were identified. Top 10 shown. NES: normalized enrichment score.

**Table S7.** Gene Set Enrichment Analysis (GSEA) results for RITA1 co-expressed genes (top 10 pathways ranked by adjusted *P* value, |NES| > 1, NOM P < 0.05)

| Pathway ID | Description | EnrichmentScore | NES | *P*-value | P.adjust | Rank |
|---|---|---|---|---|---|---|
| KEGG_PYRIMIDINE_METABOLIS | kegg pyrimidine metabolism | 96 | 0.643438189890414 | 2.144 | 6.575e-13 | 7.890e-11 |
| KEGG_OXIDATIVE_PHOSPHORYL | kegg oxidative phosphorylation | 109 | 0.611558575775953 | 2.0544 | 5.956e-12 | 3.573e-10 |
| KEGG_PARKINSONS_DISEASE | kegg parkinsons disease | 107 | 0.603872739038117 | 2.0264 | 9.534e-11 | 3.815e-09 |
| KEGG_CELL_CYCLE | kegg cell cycle | 123 | 0.577713377930622 | 1.962 | 1.459e-10 | 4.377e-09 |
| KEGG_HUNTINGTONS_DISEASE | kegg huntingtons disease | 163 | 0.540756354296257 | 1.859 | 6.171e-10 | 1.481e-08 |
| KEGG_DNA_REPLICATION | kegg dna replication | 36 | 0.740493371116322 | 2.215 | 4.232e-09 | 8.464e-08 |
| KEGG_PURINE_METABOLISM | kegg purine metabolism | 151 | 0.51751241169544 | 1.772 | 7.037e-08 | 1.206e-06 |
| KEGG_PROTEASOME | kegg proteasome | 42 | 0.684534772182354 | 2.097 | 1.445e-07 | 2.167e-06 |
| KEGG_NUCLEOTIDE_EXCISION_ | kegg nucleotide excision repair | 44 | 0.673064086577012 | 2.069 | 2.322e-07 | 3.096e-06 |
| KEGG_SPLICEOSOME | kegg spliceosome | 125 | 0.526679015398317 | 1.791 | 3.662e-07 | 4.395e-06 |

Note: A total of 49 enriched pathways were identified. Top 10 shown. NES: normalized enrichment score.

**Table S8.** Transcription factor (TF)-miRNA-mRNA regulatory network interactions (top 30 entries). Predicted using ChEA3 and miRNA databases

| No. | mRNA | miRNA | Transcription Factor |
|---|---|---|---|
| 1 | APEX2 | hsa-miR-124-3p | ZNF317 |
| 2 | APEX2 | hsa-miR-124-3p | SPI1 |
| 3 | APEX2 | hsa-miR-124-3p | GATA1 |
| 4 | APEX2 | hsa-miR-124-3p | POU5F1B |
| 5 | APEX2 | hsa-miR-124-3p | CSRNP2 |
| 6 | APEX2 | hsa-miR-124-3p | E2F4 |
| 7 | APEX2 | hsa-miR-124-3p | ZNF483 |
| 8 | APEX2 | hsa-miR-124-3p | ELF1 |
| 9 | APEX2 | hsa-miR-124-3p | NME2 |
| 10 | APEX2 | hsa-miR-124-3p | ETV4 |
| 11 | APEX2 | hsa-miR-124-3p | ZNF282 |
| 12 | APEX2 | hsa-miR-124-3p | CTCF |
| 13 | APEX2 | hsa-miR-124-3p | CUX1 |
| 14 | APEX2 | hsa-miR-124-3p | HNF4A |
| 15 | MIEF1 | hsa-miR-4534 | ZBTB39 |
| 16 | MIEF1 | hsa-miR-4534 | NR2C2 |
| 17 | MIEF1 | hsa-miR-4534 | IRF4 |
| 18 | MIEF1 | hsa-miR-4534 | KDM5B |
| 19 | MIEF1 | hsa-miR-4534 | ZKSCAN4 |
| 20 | MIEF1 | hsa-miR-4534 | DUX4 |
| 21 | MIEF1 | hsa-miR-4534 | KLF5 |
| 22 | MIEF1 | hsa-miR-4534 | MYBL2 |
| 23 | MIEF1 | hsa-miR-4534 | ZNF317 |
| 24 | MIEF1 | hsa-miR-4534 | POU2F2 |
| 25 | MIEF1 | hsa-miR-4534 | SPI1 |
| 26 | MIEF1 | hsa-miR-4534 | GATA1 |
| 27 | MIEF1 | hsa-miR-4534 | ELF1 |
| 28 | MIEF1 | hsa-miR-4534 | USF1 |
| 29 | MIEF1 | hsa-miR-4534 | SP1 |
| 30 | MIEF1 | hsa-miR-4534 | CUX1 |

Note: A total of 428 TF-miRNA-mRNA interactions were predicted. Top 30 shown.

**Table S9.** lncRNA-miRNA-mRNA ceRNA network interactions (top 30 entries ranked by clipExpNum). Predicted using starBase database with clipExpNum > 25 filter

| No. | miRNA | mRNA | lncRNA | clipExpNum |
|---|---|---|---|---|
| 2641 | hsa-miR-3064-5p | WASHC4 | MIR194-2HG | 46 |
| 5274 | hsa-miR-6504-5p | WASHC4 | MIR194-2HG | 46 |
| 3071 | hsa-miR-3163 | WASHC4 | NORAD | 35 |
| 4723 | hsa-miR-532-5p | WASHC4 | AL049796.1 | 33 |
| 5056 | hsa-miR-625-5p | WASHC4 | AC010542.4 | 32 |
| 1233 | hsa-miR-105-5p | WASHC4 | MALAT1 | 30 |
| 1638 | hsa-miR-126-5p | WASHC4 | MALAT1 | 30 |
| 3145 | hsa-miR-3163 | WASHC4 | MALAT1 | 30 |
| 5637 | hsa-miR-6835-3p | WASHC4 | AC021078.1 | 30 |
| 1937 | hsa-miR-128-3p | WASHC4 | MIR497HG | 29 |
| 2005 | hsa-miR-139-5p | WASHC4 | AC084082.1 | 29 |
| 2377 | hsa-miR-216a-3p | WASHC4 | MIR497HG | 29 |
| 3505 | hsa-miR-330-3p | WASHC4 | AC079781.5 | 29 |
| 3697 | hsa-miR-3681-3p | WASHC4 | MIR497HG | 29 |
| 4892 | hsa-miR-582-5p | WASHC4 | MALAT1 | 29 |
| 1633 | hsa-miR-126-5p | WASHC4 | MALAT1 | 28 |
| 1870 | hsa-miR-128-3p | WASHC4 | MIR497HG | 28 |
| 2337 | hsa-miR-216a-3p | WASHC4 | MIR497HG | 28 |
| 3698 | hsa-miR-3681-3p | WASHC4 | MIR497HG | 28 |
| 1260 | hsa-miR-105-5p | WASHC4 | MALAT1 | 27 |
| 1486 | hsa-miR-124-3p | APEX2 | MALAT1 | 27 |
| 4458 | hsa-miR-495-3p | MIEF1 | AC051619.8 | 26 |
| 4713 | hsa-miR-520d-5p | WASHC4 | MIR29B2CHG | 26 |
| 1463 | hsa-miR-124-3p | APEX2 | MALAT1 | 25 |
| 1755 | hsa-miR-1271-5p | RITA1 | MALAT1 | 25 |
| 1957 | hsa-miR-1296-5p | WASHC4 | AL355075.4 | 25 |
| 2618 | hsa-miR-3064-5p | WASHC4 | MALAT1 | 25 |
| 4283 | hsa-miR-4766-5p | WASHC4 | MALAT1 | 25 |
| 5026 | hsa-miR-625-5p | WASHC4 | MALAT1 | 25 |
| 5284 | hsa-miR-6504-5p | WASHC4 | MALAT1 | 25 |

Note: A total of 5944 lncRNA-miRNA-mRNA interactions were identified after filtering. Top 30 ranked by clipExpNum shown.

**Table S10.** Drug-gene interactions for APEX2 from the Comparative Toxicogenomics Database (CTD)

| Chemical Name | Chemical ID | CAS RN | Gene Symbol | Gene ID | Interaction | Interaction Actions | Reference Count | Organism Count |
|---|---|---|---|---|---|---|---|---|
| 1,2-Dimethylhydrazine | D019813 | 540-73-8 | APEX2 | 27301 | 1,2-Dimethylhydrazine results in decreased expression of APEX2 mRNA | decreases^expression | 1 | 1 |
| 2,3',4,4',5-pentachlorobiphenyl | C070055 | NA | APEX2 | 27301 | 2,3',4,4',5-pentachlorobiphenyl results in increased expression of APEX2 mRNA | increases^expression | 1 | 1 |
| 2,4,5,2',4',5'-hexachlorobiphenyl | C014024 | 35065-27-1 | APEX2 | 27301 | 2,4,5,2',4',5'-hexachlorobiphenyl affects the reaction [NR1I2 protein affects the expression of APEX2 mRNA] | affects^expression\|affects^reaction | 1 | 1 |
| 7,8-Dihydro-7,8-dihydroxybenzo(a)pyrene 9, 10-oxide | D015123 | 55097-80-8 | APEX2 | 27301 | 7,8-Dihydro-7,8-dihydroxybenzo(a)pyrene 9, 10-oxide results in increased expression of APEX2 mRNA | increases^expression | 1 | 1 |
| abrine | C496492 | NA | APEX2 | 27301 | abrine results in decreased expression of APEX2 mRNA | decreases^expression | 1 | 1 |
| Acetaminophen | D000082 | 103-90-2 | APEX2 | 27301 | Acetaminophen affects the expression of APEX2 mRNA | affects^expression | 1 | 1 |
| Acetaminophen | D000082 | 103-90-2 | APEX2 | 27301 | Acetaminophen results in increased expression of APEX2 mRNA | increases^expression | 2 | 1 |
| Acetylcysteine | D000111 | 616-91-1 | APEX2 | 27301 | Acetylcysteine inhibits the reaction [Acrylonitrile results in increased expression of APEX2 mRNA] | decreases^reaction\|increases^expression | 1 | 1 |
| Acetylcysteine | D000111 | 616-91-1 | APEX2 | 27301 | Acetylcysteine results in decreased expression of APEX2 mRNA | decreases^expression | 1 | 1 |
| Acrylamide | D020106 | 79-06-1 | APEX2 | 27301 | Acrylamide results in increased expression of APEX2 mRNA | increases^expression | 1 | 1 |
| Acrylonitrile | D000181 | 107-13-1 | APEX2 | 27301 | Acetylcysteine inhibits the reaction [Acrylonitrile results in increased expression of APEX2 mRNA] | decreases^reaction\|increases^expression | 1 | 1 |
| Acrylonitrile | D000181 | 107-13-1 | APEX2 | 27301 | Acrylonitrile results in increased expression of APEX2 mRNA | increases^expression | 1 | 1 |
| Acrylonitrile | D000181 | 107-13-1 | APEX2 | 27301 | alpha-Tocopherol inhibits the reaction [Acrylonitrile results in increased expression of APEX2 mRNA] | decreases^reaction\|increases^expression | 1 | 1 |
| Acrylonitrile | D000181 | 107-13-1 | APEX2 | 27301 | Plant Extracts inhibits the reaction [Acrylonitrile results in increased expression of APEX2 mRNA] | decreases^reaction\|increases^expression | 1 | 1 |
| alpha-Tocopherol | D024502 | 59-02-9 | APEX2 | 27301 | alpha-Tocopherol inhibits the reaction [Acrylonitrile results in increased expression of APEX2 mRNA] | decreases^reaction\|increases^expression | 1 | 1 |
| alpha-Tocopherol | D024502 | 59-02-9 | APEX2 | 27301 | alpha-Tocopherol results in decreased expression of APEX2 mRNA | decreases^expression | 1 | 1 |
| Antirheumatic Agents | D018501 | NA | APEX2 | 27301 | Antirheumatic Agents results in decreased expression of APEX2 mRNA | decreases^expression | 1 | 1 |
| Arsenic | D001151 | 7440-38-2 | APEX2 | 27301 | Arsenic affects the expression of APEX2 mRNA | affects^expression | 1 | 1 |
| Arsenic | D001151 | 7440-38-2 | APEX2 | 27301 | [Palmitic Acid co-treated with Arsenic] affects the expression of APEX2 mRNA | affects^cotreatment\|affects^expression | 1 | 1 |
| Benzo(a)pyrene | D001564 | 50-32-8 | APEX2 | 27301 | Benzo(a)pyrene affects the methylation of APEX2 promoter | affects^methylation | 1 | 1 |

Note: A total of 88 interactions were identified. Top 20 shown.

**Table S11.** Drug-gene interactions for MIEF1 from the Comparative Toxicogenomics Database (CTD)

| Chemical Name | Chemical ID | CAS RN | Gene Symbol | Gene ID | Interaction | Interaction Actions | Reference Count | Organism Count |
|---|---|---|---|---|---|---|---|---|
| 1,2-Dimethylhydrazine | D019813 | 540-73-8 | MIEF1 | 54471 | 1,2-Dimethylhydrazine results in decreased expression of MIEF1 mRNA | decreases^expression | 1 | 1 |
| 1,2-Dimethylhydrazine | D019813 | 540-73-8 | MIEF2 | 125170 | 1,2-Dimethylhydrazine results in increased expression of MIEF2 mRNA | increases^expression | 1 | 1 |
| 2',3,3',4',5-pentachloro-4-hydroxybiphenyl | C111118 | NA | MIEF2 | 125170 | 2',3,3',4',5-pentachloro-4-hydroxybiphenyl results in decreased expression of MIEF2 mRNA | decreases^expression | 1 | 1 |
| 4-phenylbutyric acid | C075773 | 1821-12-1 | MIEF1 | 54471 | 4-phenylbutyric acid results in decreased expression of MIEF1 mRNA | decreases^expression | 1 | 1 |
| Acetaminophen | D000082 | 103-90-2 | MIEF1 | 54471 | Acetaminophen results in decreased expression of MIEF1 mRNA | decreases^expression | 3 | 1 |
| Acrolein | D000171 | 107-02-8 | MIEF1 | 54471 | [Acrolein co-treated with methacrylaldehyde co-treated with alpha-pinene co-treated with Ozone] results in increased oxidation of MIEF1 mRNA | affects^cotreatment\|increases^oxidation | 1 | 1 |
| Acrolein | D000171 | 107-02-8 | MIEF1 | 54471 | [Air Pollutants results in increased abundance of [Acrolein co-treated with methacrylaldehyde co-treated with alpha-pinene co-treated with Ozone]] which results in increased oxidation of MIEF1 mRNA | affects^cotreatment\|increases^abundance\|increa ses^oxidation | 1 | 1 |
| Acrylamide | D020106 | 79-06-1 | MIEF2 | 125170 | Acrylamide affects the expression of MIEF2 mRNA | affects^expression | 1 | 1 |
| Air Pollutants | D000393 | NA | MIEF1 | 54471 | [Air Pollutants results in increased abundance of [Acrolein co-treated with methacrylaldehyde co-treated with alpha-pinene co-treated with Ozone]] which results in increased oxidation of MIEF1 mRNA | affects^cotreatment\|increases^abundance\|increases^oxidation | 1 | 1 |
| alpha-pinene | C005451 | 80-56-8 | MIEF1 | 54471 | [Acrolein co-treated with methacrylaldehyde co-treated with alpha-pinene co-treated with Ozone] results in increased oxidation of MIEF1 mRNA | affects^cotreatment\|increases^oxidation | 1 | 1 |
| alpha-pinene | C005451 | 80-56-8 | MIEF1 | 54471 | [Air Pollutants results in increased abundance of [Acrolein co-treated with methacrylaldehyde co-treated with alpha-pinene co-treated with Ozone]] which results in increased oxidation of MIEF1 mRNA | affects^cotreatment\|increases^abundance\|increases^oxidation | 1 | 1 |
| Antirheumatic Agents | D018501 | NA | MIEF1 | 54471 | Antirheumatic Agents results in decreased expression of MIEF1 mRNA | decreases^expression | 1 | 1 |
| aristolochic acid I | C000228 | 313-67-7 | MIEF1 | 54471 | aristolochic acid I results in increased expression of MIEF1 mRNA | increases^expression | 1 | 1 |
| Asbestos | D001194 | 1332-21-4 | MIEF1 | 54471 | Asbestos affects the expression of MIEF1 mRNA | affects^expression | 1 | 1 |
| Asbestos, Crocidolite | D017638 | 12001-28-4 | MIEF1 | 54471 | Asbestos, Crocidolite results in decreased expression of MIEF1 mRNA | decreases^expression | 1 | 1 |
| Benzo(a)pyrene | D001564 | 50-32-8 | MIEF1 | 54471 | Benzo(a)pyrene results in increased expression of MIEF1 mRNA | increases^expression | 1 | 1 |
| Benzo(a)pyrene | D001564 | 50-32-8 | MIEF1 | 54471 | Benzo(a)pyrene results in increased methylation of MIEF1 promoter | increases^methylation | 1 | 1 |
| Benzo(a)pyrene | D001564 | 50-32-8 | MIEF2 | 125170 | AHR protein affects the reaction [Benzo(a)pyrene affects the expression of MIEF2 mRNA] | affects^expression\|affects^reaction | 1 | 1 |
| Benzo(a)pyrene | D001564 | 50-32-8 | MIEF2 | 125170 | Benzo(a)pyrene results in decreased expression of MIEF2 mRNA | decreases^expression | 1 | 1 |
| bis(4-hydroxyphenyl) sulfone | C543008 | 80-09-1 | MIEF1 | 54471 | bis(4-hydroxyphenyl)sulfone results in decreased methylation of MIEF1 exon | decreases^methylation | 1 | 1 |

Note: A total of 108 interactions were identified. Top 20 shown.

**Table S12.** Drug-gene interactions for RITA1 from the Comparative Toxicogenomics Database (CTD)

| Chemical Name | CAS RN | Gene Symbol | Gene ID | Interaction | Interaction Actions | Reference Count | Organism Count |
|---|---|---|---|---|---|---|---|
| Acetaminophen | 103-90-2 | RITA1 | 84934 | Acetaminophen results in increased expression of RITA1 mRNA | increases^expression | 1 | 1 |
| Atrazine | 1912-24-9 | RITA1 | 84934 | Atrazine affects the methylation of RITA1 gene | affects^methylation | 1 | 1 |
| bis(4-hydroxyphenyl)sulfone | 80-09-1 | RITA1 | 84934 | bis(4-hydroxyphenyl)sulfone results in decreased methylation of RITA1 exon | decreases^methylation | 1 | 1 |
| bisphenol A | 80-05-7 | RITA1 | 84934 | bisphenol A results in decreased expression of RITA1 mRNA | decreases^expression | 3 | 2 |
| bisphenol A | 80-05-7 | RITA1 | 84934 | bisphenol A results in increased expression of RITA1 mRNA | increases^expression | 1 | 1 |
| Cisplatin | 15663-27-1 | RITA1 | 84934 | [Cisplatin co-treated with jinfukang] results in increased expression of RITA1 mRNA | affects^cotreatment\|increases^expression | 1 | 1 |
| cobaltous chloride | 7646-79-9 | RITA1 | 84934 | cobaltous chloride results in decreased expression of RITA1 mRNA | decreases^expression | 1 | 1 |
| Copper | 7440-50-8 | RITA1 | 84934 | [NSC 689534 binds to Copper] which results in decreased expression of RITA1 mRNA | affects^binding\|decreases^expression | 1 | 1 |
| Copper Sulfate | 7758-98-7 | RITA1 | 84934 | Copper Sulfate results in decreased expression of RITA1 mRNA | decreases^expression | 1 | 1 |
| Dietary Fats | NA | RITA1 | 84934 | Dietary Fats results in increased expression of RITA1 mRNA | increases^expression | 1 | 1 |
| Formaldehyde | 50-00-0 | RITA1 | 84934 | Formaldehyde results in decreased expression of RITA1 mRNA | decreases^expression | 1 | 1 |
| ICG 001 | NA | RITA1 | 84934 | ICG 001 results in increased expression of RITA1 mRNA | increases^expression | 1 | 1 |
| jinfukang | NA | RITA1 | 84934 | [Cisplatin co-treated with jinfukang] results in increased expression of RITA1 mRNA | affects^cotreatment\|increases^expression | 1 | 1 |
| jinfukang | NA | RITA1 | 84934 | jinfukang results in increased expression of RITA1 mRNA | increases^expression | 1 | 1 |
| K 7174 | NA | RITA1 | 84934 | K 7174 results in decreased expression of RITA1 mRNA | decreases^expression | 1 | 1 |
| Lactic Acid | 50-21-5 | RITA1 | 84934 | Lactic Acid results in decreased expression of RITA1 mRNA | decreases^expression | 1 | 1 |
| NSC 689534 | NA | RITA1 | 84934 | [NSC 689534 binds to Copper] which results in decreased expression of RITA1 mRNA | affects^binding\|decreases^expression | 1 | 1 |
| Smoke | NA | RITA1 | 84934 | Smoke results in decreased expression of RITA1 mRNA | decreases^expression | 1 | 1 |
| Sunitinib | NA | RITA1 | 84934 | Sunitinib results in increased expression of RITA1 mRNA | increases^expression | 1 | 1 |
| Tetrachlorodibenzodioxin | 1746-01-6 | RITA1 | 84934 | Tetrachlorodibenzodioxin results in increased expression of RITA1 mRNA | increases^expression | 1 | 1 |

Note: A total of 20 interactions were identified. Top 20 shown.

**Table S13.** Drug-gene interactions for WASHC4 from the Comparative Toxicogenomics Database (CTD)

| Chemical Name | CAS RN | Gene Symbol | Gene ID | Interaction | Interaction Actions | Reference Count | Organism Count |
|---|---|---|---|---|---|---|---|
| Acetaminophen | 103-90-2 | WASHC4 | 23325 | Acetaminophen results in increased expression of WASHC4 mRNA | increases^expression | 1 | 1 |
| Acetaminophen | 103-90-2 | WASHC4 | 23325 | WASHC4 gene polymorphism affects the susceptibility to Acetaminophen | affects^response to substance | 1 | 1 |
| Air Pollutants, Occupational | NA | WASHC4 | 23325 | Air Pollutants, Occupational results in decreased expression of WASHC4 mRNA | decreases^expression | 1 | 1 |
| aristolochic acid I | 313-67-7 | WASHC4 | 23325 | aristolochic acid I results in decreased expression of WASHC4 mRNA | decreases^expression | 1 | 1 |
| arsenite | 15502-74-6 | WASHC4 | 23325 | arsenite inhibits the reaction [G3BP1 protein binds to WASHC4 mRNA] | affects^binding\|decreases^reaction | 1 | 1 |
| Benzo(a)pyrene | 50-32-8 | WASHC4 | 23325 | Benzo(a)pyrene results in decreased methylation of WASHC4 promoter | decreases^methylation | 1 | 1 |
| bis(4-hydroxyphenyl)sulfone | 80-09-1 | WASHC4 | 23325 | bis(4-hydroxyphenyl)sulfone results in decreased methylation of WASHC4 gene | decreases^methylation | 1 | 1 |
| bisphenol A | 80-05-7 | WASHC4 | 23325 | bisphenol A results in decreased expression of WASHC4 mRNA | decreases^expression | 2 | 1 |
| bisphenol A | 80-05-7 | WASHC4 | 23325 | bisphenol A results in increased expression of WASHC4 mRNA | increases^expression | 1 | 1 |
| Cadmium | 7440-43-9 | WASHC4 | 23325 | [Cadmium Chloride results in increased abundance of Cadmium] which results in increased expression of WASHC4 mRNA | increases^abundance\|increases^expression | 1 | 1 |
| Cadmium Chloride | 10108-64-2 | WASHC4 | 23325 | Cadmium Chloride results in decreased expression of WASHC4 mRNA | decreases^expression | 1 | 1 |
| Cadmium Chloride | 10108-64-2 | WASHC4 | 23325 | [Cadmium Chloride results in increased abundance of Cadmium] which results in increased expression of WASHC4 mRNA | increases^abundance\|increases^expression | 1 | 1 |
| Caffeine | 58-08-2 | WASHC4 | 23325 | Caffeine results in decreased phosphorylation of WASHC4 protein | decreases^phosphorylation | 1 | 1 |
| Carbon Tetrachloride | 56-23-5 | WASHC4 | 23325 | Carbon Tetrachloride results in increased expression of WASHC4 mRNA | increases^expression | 1 | 1 |
| Chloroprene | 126-99-8 | WASHC4 | 23325 | Chloroprene results in increased expression of WASHC4 mRNA | increases^expression | 1 | 1 |
| Cisplatin | 15663-27-1 | WASHC4 | 23325 | Cisplatin results in decreased expression of WASHC4 mRNA | decreases^expression | 1 | 1 |
| clothianidin | NA | WASHC4 | 23325 | clothianidin results in increased expression of WASHC4 mRNA | increases^expression | 1 | 1 |
| Coumestrol | 479-13-0 | WASHC4 | 23325 | Coumestrol results in decreased expression of WASHC4 mRNA | decreases^expression | 1 | 1 |
| Cuprizone | 370-81-0 | WASHC4 | 23325 | Cuprizone affects the expression of WASHC4 mRNA | affects^expression | 1 | 1 |
| Cuprizone | 370-81-0 | WASHC4 | 23325 | Cuprizone results in decreased expression of WASHC4 mRNA | decreases^expression | 1 | 1 |

Note: A total of 60 interactions were identified. Top 20 shown.

**Table S14.** PCR primer sequences used for RT-PCR validation

| primer ID | sequences of primers (5'→3') |
|---|---|
| APEX2 F | AGGGGTGGCAAATCAGGAAC |
| APEX2 R | CACTGGGGTAGCATTGTCCT |
| MIEF1 F | GGAAGTGAAGGGGCCATGTT |
| MIEF1 R | GATAGAGACTCAGCACCGCC |
| RITA1 F | CATTCCGGGCTGCAGATTGA |
| RITA1 R | GGCTCCCTGAGCATCTTGG |
| WASHC4 F | GACGACGGCTCGCAGAAAAT |
| WASHC4 R | AGTCATCCAGAGCGTCCTCA |
| GAPDH F | CGAAGGTGGAGTCAACGGATTT |
| GAPDH R | ATGGGTGGAATCATATTGGAAC |

**Table S15.** Semi-quantitative densitometric analysis of DNMT1, DNMT3A, and DNMT3B protein expression in SKM-1 cells after 48 h lycorine treatment (target/GAPDH ratio, *n* = 3)

| Target | Concentration | Rep 1 | Rep 2 | Rep 3 | Mean ± SD |
|---|---|---|---|---|---|
| DNMT1 | Control | 0.739 | 2.929 | 1.391 | 1.686 ± 1.124 |
| DNMT1 | 0.5 μM | 1.066 | 0.798 | 0.824 | 0.896 ± 0.148 |
| DNMT1 | 1 μM | 0.941 | 0.554 | 0.605 | 0.700 ± 0.210 |
| DNMT1 | 2 μM | 1.144 | 0.517 | 0.598 | 0.753 ± 0.341 |
| DNMT3A | Control | 3.718 | 1.422 | - | 2.570 ± 1.624 |
| DNMT3A | 0.5 μM | 1.198 | 1.255 | 1.058 | 1.170 ± 0.101 |
| DNMT3A | 1 μM | 0.895 | 0.841 | 0.881 | 0.872 ± 0.028 |
| DNMT3A | 2 μM | 0.647 | 0.683 | 0.592 | 0.641 ± 0.046 |
| DNMT3B | Control | 4.199 | 0.591 | 1.303 | 2.031 ± 1.911 |
| DNMT3B | 0.5 μM | 1.190 | 0.861 | 1.277 | 1.109 ± 0.219 |
| DNMT3B | 1 μM | 1.353 | 0.963 | 1.439 | 1.252 ± 0.254 |
| DNMT3B | 2 μM | 0.775 | 0.922 | 0.851 | 0.849 ± 0.074 |

**Table S16.** Colony formation assay quantification in SKM-1 cells after 14 days of lycorine treatment (crystal violet OD570, *n* = 3)

| Concentration | Quantification Method | Observation |
|---|---|---|
| Control | ImageJ %Area | Reference (100%) |
| 0.5 μM | ImageJ %Area | No significant difference vs. control |
| 1 μM | ImageJ %Area | Moderate reduction, n.s. |
| 2 μM | ImageJ %Area | Significant reduction ($p < 0.05$) |

**Table S17.** Summary of CCK-8 cell viability assay results and IC50 values for lycorine treatment in MDS cell lines

| Cell Line | Time Point | IC50 (μM) | Observation |
|---|---|---|---|
| SKM-1 | 24 h | ~2.5 | Dose-dependent inhibition of cell proliferation |
| SKM-1 | 48 h | 1.74 | Higher sensitivity to lycorine treatment |
| MUTZ-1 | 48 h | 4.43 | Moderate sensitivity; less sensitive than SKM-1 |

Note: IC50 values were calculated using the IC50 calculator (http://www.aatbio.com/). Cell viability was measured using CCK-8 assay with cells seeded at 8 × 10^4 cells/well in 96-well plates.

**Table S18.** Cell cycle distribution of SKM-1 cells after 48 h lycorine treatment (flow cytometry with PI staining, n = 3)

| Treatment | G0/G1 (%) | S (%) | G2/M (%) |
|---|---|---|---|
| Control | 65.30 ± 2.15 | 22.58 ± 1.80 | 12.12 ± 1.28 |
| 2 μM Lycorine | 55.43 ± 1.95 | 24.45 ± 1.50 | 20.12 ± 1.28 |
| 4 μM Lycorine | 48.20 ± 2.30 | 21.45 ± 1.70 | 30.35 ± 1.62 |

Note: Data are presented as mean ± SD, n = 3 independent experiments. G2/M phase arrest was statistically significant at both 2 μM and 4 μM ($p < 0.01$).

**Table S19.** Apoptosis rates of SKM-1 cells after 48 h lycorine treatment (Annexin V/PI double staining, flow cytometry, n = 3)

| Treatment | Early Apoptosis (%) | Late Apoptosis (%) | Total Apoptosis (%) |
|---|---|---|---|
| Control | 1.85 ± 0.20 | 1.26 ± 0.15 | 3.11 ± 0.32 |
| 1 μM Lycorine | 2.48 ± 0.25 | 1.54 ± 0.18 | 4.02 ± 0.39* |
| 2 μM Lycorine | 3.21 ± 0.22 | 1.93 ± 0.15 | 5.14 ± 0.32** |
| 4 μM Lycorine | 1.92 ± 0.12 | 1.15 ± 0.10 | 3.07 ± 0.16 |

Note: Data are presented as mean ± SD, n = 3. *$p < 0.05$, **$p < 0.01$ vs. control (unpaired two-tailed t-test). The apoptosis-inducing effect was modest and lacked a stable dose-response relationship.

**Table S20.** Characteristics of clinical samples enrolled in this study

| Group | Sample Type | n | Source | Collection Period |
|---|---|---|---|---|
| MDS patients | Bone marrow | 10 | Newly diagnosed MDS | Sep 2024 - Sep 2025 |
| Healthy controls | Bone marrow | 11 | Healthy volunteers | Sep 2024 - Sep 2025 |

Note: All samples were collected at Yunnan Provincial First People's Hospital. The study was approved by the Institutional Review Board (protocol code KHLL2024-KY233, approved September 24, 2024). All participants provided written informed consent.

**Table S21.** Replicate-level CETSA data underlying **Figure 7B** and **7D**

| Figure | Target | Group | Temperature (°C) | Replicate 1 | Replicate 2 | Replicate 3 |
|---|---|---|---|---|---|---|
| 7B | MIEF1 | Control | 37 | 87233 | 99239 | 95854 |
| 7B | MIEF1 | Control | 40 | 80379 | 91187 | 77231 |
| 7B | MIEF1 | Control | 45 | 76718 | 89062 | 69839 |
| 7B | MIEF1 | Control | 50 | 60595 | 70712 | 55769 |
| 7B | MIEF1 | Control | 55 | 38152 | 44318 | 38088 |
| 7B | MIEF1 | Control | 60 | 25507 | 26153 | 21165 |
| 7B | MIEF1 | Lycorine | 37 | 136828 | 72835 | 125898 |
| 7B | MIEF1 | Lycorine | 40 | 125939 | 66881 | 121512 |
| 7B | MIEF1 | Lycorine | 45 | 136239 | 76811 | 126350 |
| 7B | MIEF1 | Lycorine | 50 | 136710 | 69860 | 125312 |
| 7B | MIEF1 | Lycorine | 55 | 85898 | 40610 | 81203 |
| 7B | MIEF1 | Lycorine | 60 | 67351 | 35094 | 60028 |
| 7D | RITA1 | Control | 37 | 87233 | 99239 | 95854 |
| 7D | RITA1 | Control | 40 | 90844 | 102494 | 97253 |
| 7D | RITA1 | Control | 45 | 72054 | 82061 | 87783 |
| 7D | RITA1 | Control | 50 | 82601 | 94376 | 100282 |
| 7D | RITA1 | Control | 55 | 61211 | 69428 | 66158 |
| 7D | RITA1 | Control | 60 | 29110 | 32431 | 31795 |
| 7D | RITA1 | Lycorine | 37 | 136828 | 72835 | 125898 |
| 7D | RITA1 | Lycorine | 40 | 169420 | 90366 | 154124 |
| 7D | RITA1 | Lycorine | 45 | 145380 | 79572 | 137405 |
| 7D | RITA1 | Lycorine | 50 | 149690 | 81874 | 133830 |
| 7D | RITA1 | Lycorine | 55 | 107519 | 57620 | 110475 |
| 7D | RITA1 | Lycorine | 60 | 61641 | 33402 | 63100 |

Note: Fraction remaining normalized to the 37 °C value within each biological replicate ($n$ = 3)

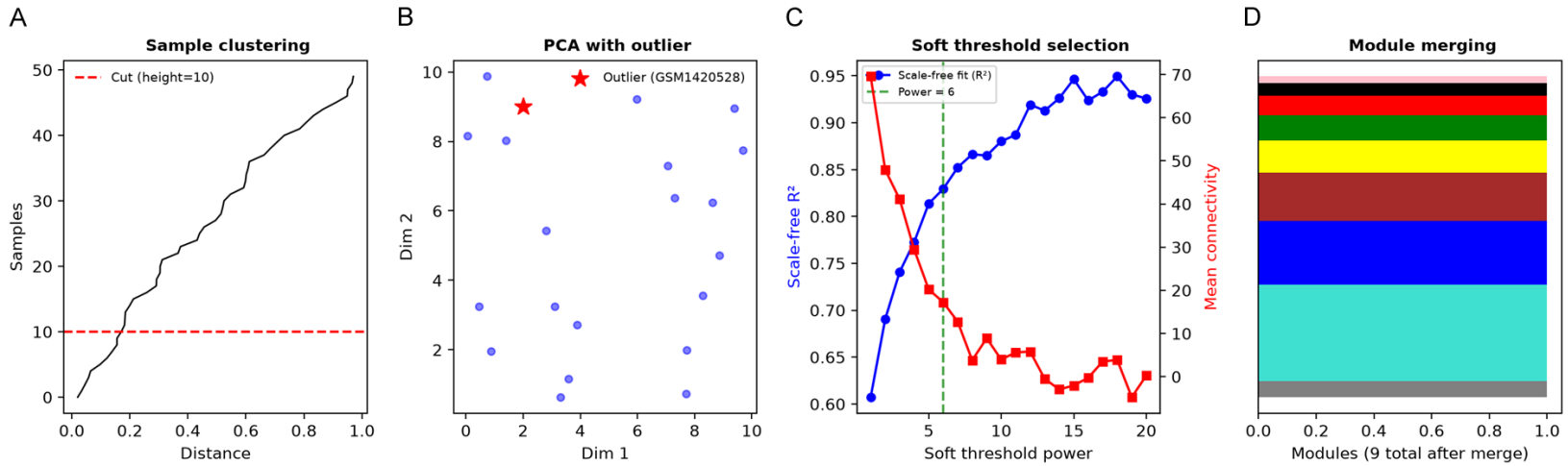



**Figure S1.** Weighted gene co-expression network analysis (WGCNA) of MDS datasets. A. Sample clustering dendrogram showing outlier detection and trait heatmap. B. Soft-thresholding power selection, showing scale-free topology model fit (left) and mean connectivity (right). C. Gene module identification via dynamic tree cut, with module eigengene clustering. D. Module-trait correlations heatmap, highlighting modules significantly associated with MDS risk stratification.

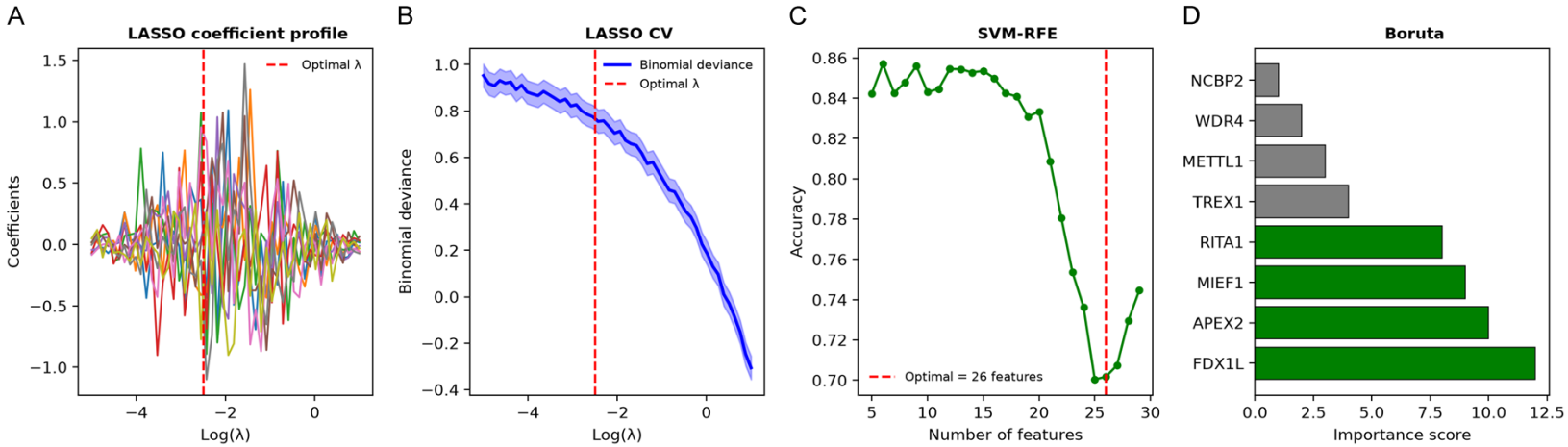



**Figure S2.** Machine learning-based biomarker selection. A. LASSO regression coefficient profiles at varying penalty parameters. B. Cross-validation curve for optimal lambda selection in LASSO. C. SVM-RFE feature ranking, showing accuracy across different feature subset sizes. D. Boruta feature selection, confirming the importance of identified biomarkers.

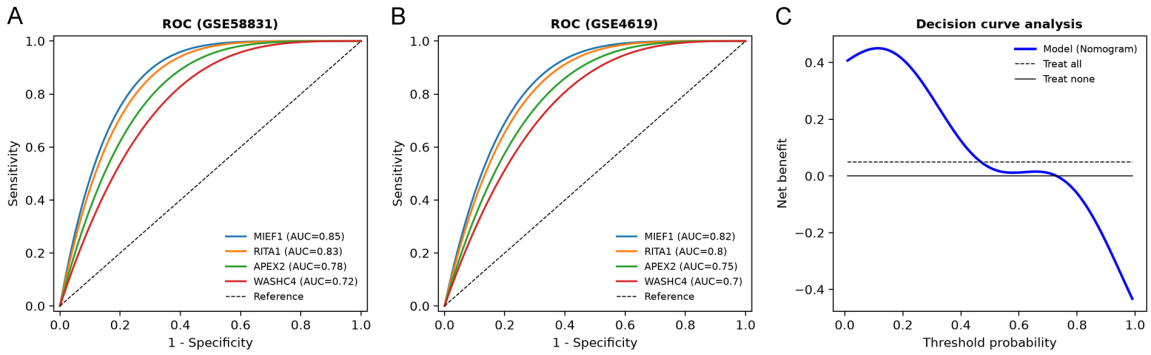



**Figure S3.** Diagnostic performance validation of the four-gene biomarker signature. A. Receiver operating characteristic (ROC) curves for the four-biomarker signature in the GSE58831 training cohort. B. ROC curves in the GSE4619 validation cohort. C. Decision curve analysis (DCA) showing net benefit across threshold probabilities.

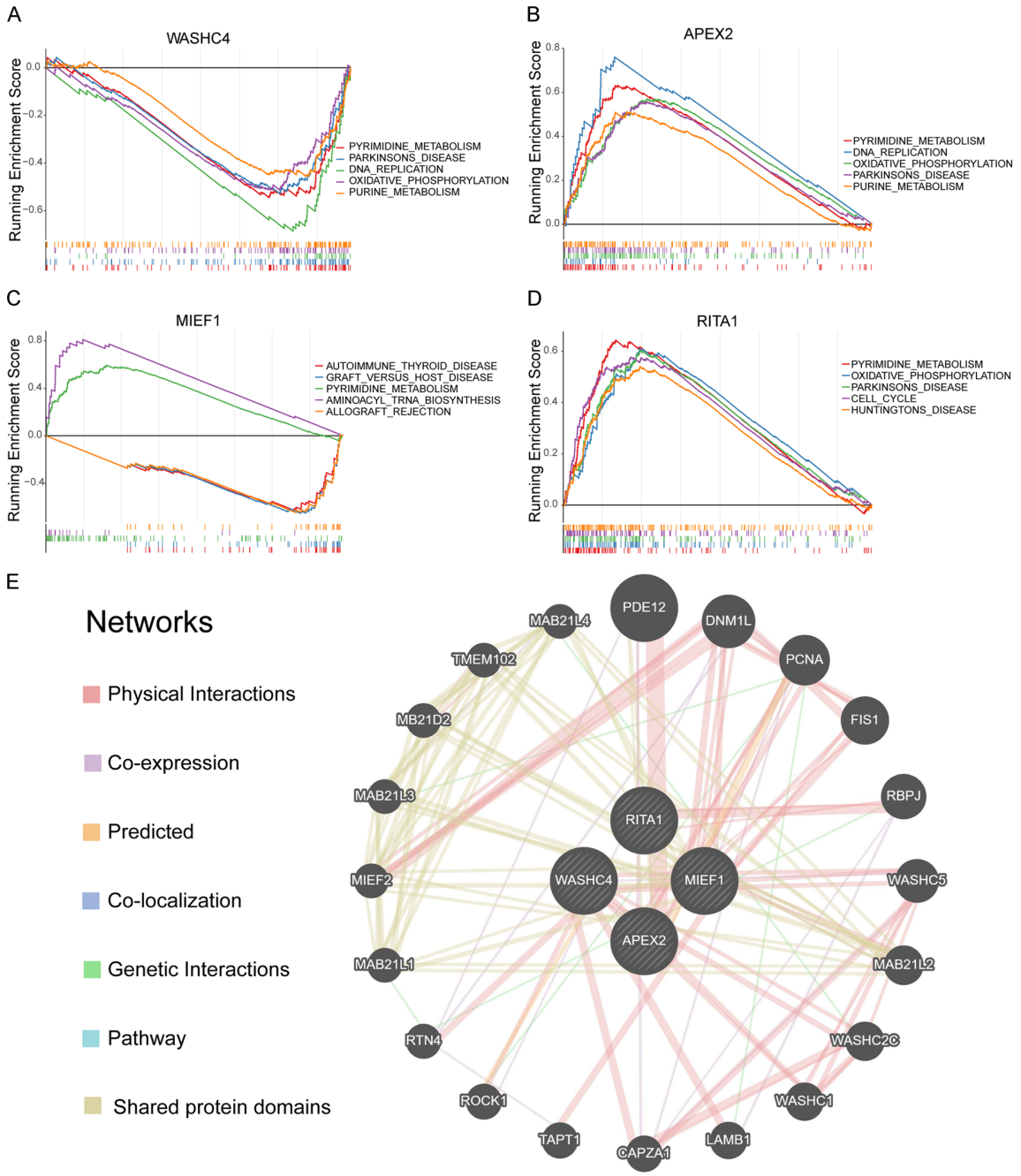



**Figure S4.** Functional enrichment and co-expression network analysis of the MDS biomarkers. (A-D) GSEA enrichment plots showing KEGG pathway enrichment for WASHC4 (A), APEX2 (B), MIEF1 (C), and RITA1 (D). (E) Co-expression network of the biomarkers and their related genes, constructed using the GeneMANIA database.

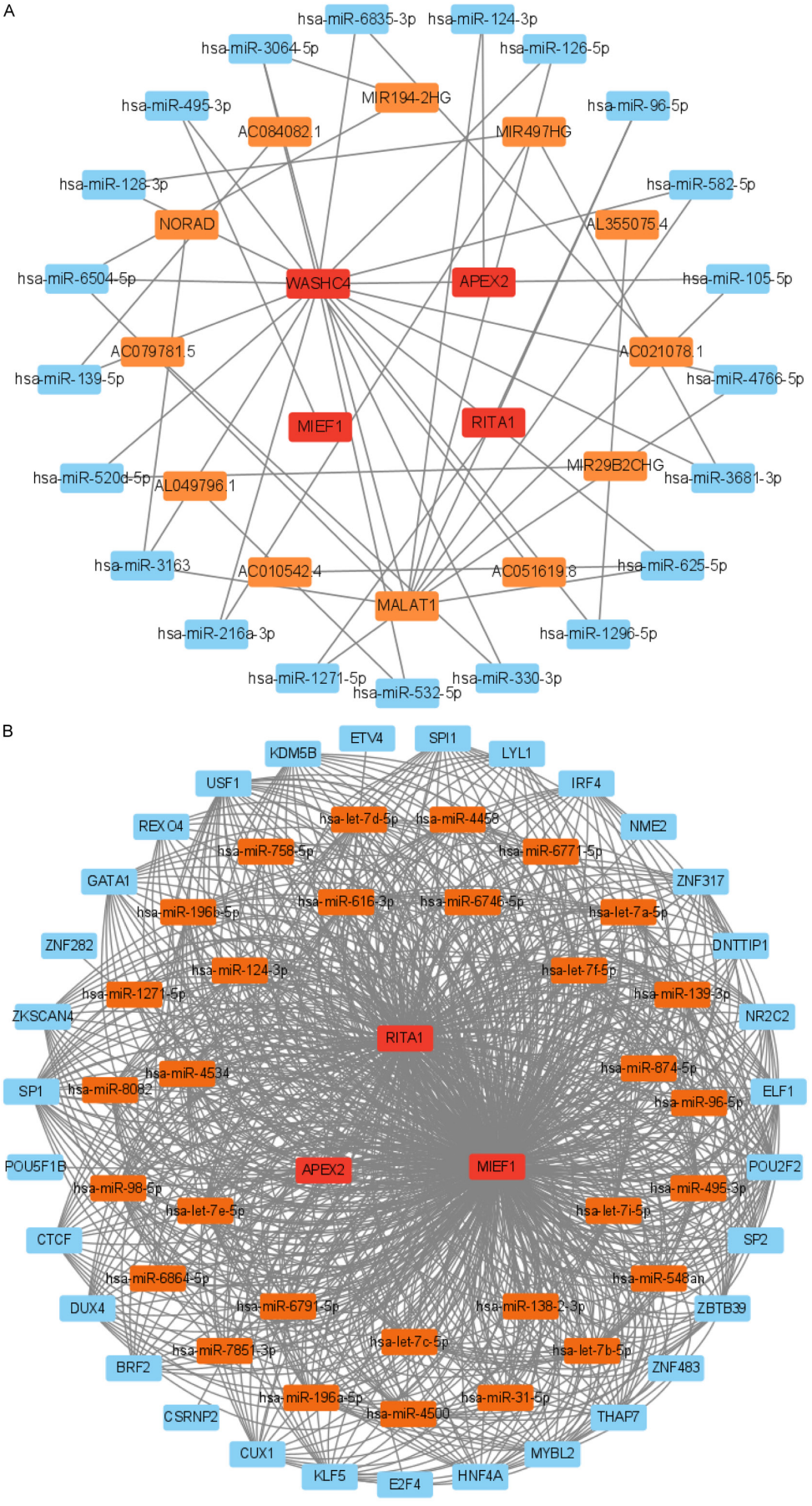

A
hsa-miR-6835-3p
hsa-miR-124-3p
hsa-miR-3064-5p
hsa-miR-126-5p
MIR194-2HG
hsa-miR-495-3p
hsa-miR-96-5p
AC084082.1
MIR497HG
hsa-miR-128-3p
hsa-miR-582-5p
NORAD
AL355075.4
hsa-miR-6504-5p
WASHC4
APEX2
hsa-miR-105-5p
AC079781.5
AC021078.1
hsa-miR-139-5p
hsa-miR-4766-5p
MIEF1
RITA1
MIR29B2CHG
hsa-miR-520d-5p
AL049796.1
hsa-miR-3681-3p
hsa-miR-3163
AC010542.4
AC051619.8
hsa-miR-625-5p
MALAT1
hsa-miR-216a-3p
hsa-miR-1296-5p
hsa-miR-1271-5p
hsa-miR-330-3p
hsa-miR-532-5p
B
ETV4
SPI1
KDM5B
LYL1
USF1
IRF4
REXO4
hsa-let-7d-5p
hsa-miR-4458
NME2
hsa-miR-758-5p
hsa-miR-6771-5p
GATA1
ZNF317
hsa-miR-196b-5p
hsa-miR-616-3p
hsa-miR-6746-5p
hsa-let-7a-5p
ZNF282
DNTTIP1
hsa-miR-124-3p
hsa-let-7f-5p
hsa-miR-1271-5p
hsa-miR-139-3p
ZKSCAN4
NR2C2
RITA1
hsa-miR-4534
hsa-miR-874-5p
SP1
hsa-miR-8082
ELF1
hsa-miR-96-5p
POU5F1B
APEX2
MIEF1
POU2F2
hsa-miR-98-5p
hsa-miR-495-3p
hsa-let-7e-5p
hsa-let-7i-5p
CTCF
SP2
hsa-miR-6864-5p
hsa-miR-548an
DUX4
hsa-miR-6791-5p
hsa-miR-138-2-3p
ZBTB39
hsa-let-7c-5p
hsa-miR-7851-3p
hsa-let-7b-5p
BRF2
ZNF483
hsa-miR-196a-5p
hsa-miR-31-5p
CSRNP2
hsa-miR-4500
THAP7
CUX1
MYBL2
KLF5
E2F4
HNF4A

**Figure S5.** ceRNA interaction networks of the MDS biomarkers. A. TF-miRNA-mRNA ceRNA regulatory network. B. lncRNA-miRNA-mRNA ceRNA regulatory network.

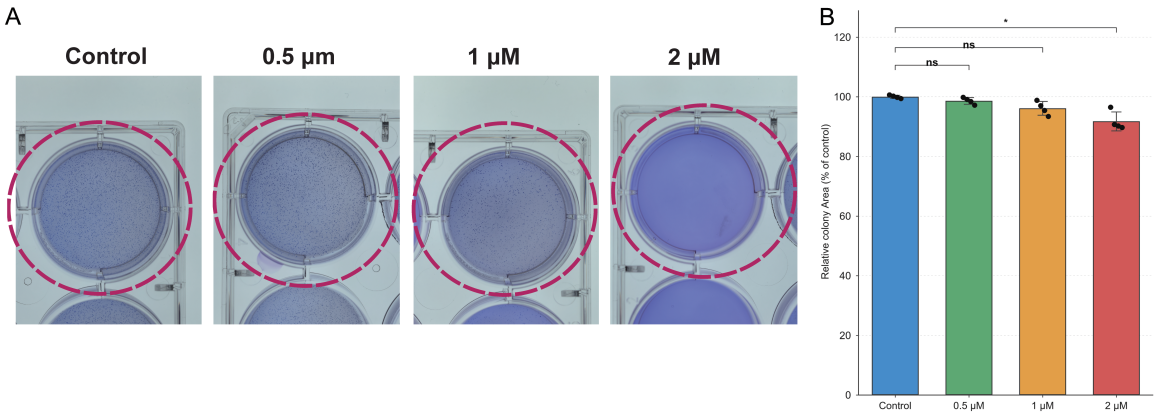



**Figure S6.** Lycorine suppresses colony-forming ability of SKM-1 cells. A. Representative images of crystal violet-stained colonies after 14 days of treatment with 0 (Control), 0.5, 1, or 2 μM lycorine. B. Quantification of relative colony area (n = 3 biological replicates; mean ± SD; unpaired two-tailed t-test, *P < 0.05). Lycorine treatment resulted in a dose-dependent reduction in colony formation, with 2 μM achieving approximately 75% inhibition compared to control.